

Bonding, Structure, and Energetics of Gaseous E_8^{2+} and of Solid $E_8(AsF_6)_2$ ($E = S, Se$)[†]

T. Stanley Cameron,^{*,‡} Robert J. Deeth,[§] Isabelle Dionne,^{||} Hongbin Du,^{||}
H. Donald B. Jenkins,^{*,§} Ingo Crossing,^{*,⊥} Jack Passmore,^{*,||} and Helen K. Roobottom[§]

Departments of Chemistry, Dalhousie University, Halifax, Nova Scotia, Canada B3H 4J3, University of Warwick, Coventry CV4 7AL, West Midlands, U.K., University of New Brunswick, Fredericton, New Brunswick, Canada E3B 6E2, and University of Karlsruhe, 76128 Karlsruhe, Germany

Received June 30, 1999

The attempt to prepare hitherto unknown homopolyatomic cations of sulfur by the reaction of elemental sulfur with *blue* $S_8(AsF_6)_2$ in liquid SO_2/SO_2ClF , led to *red* (in transmitted light) crystals identified crystallographically as $S_8(AsF_6)_2$. The X-ray structure of this salt was redetermined with improved resolution and corrected for librational motion: monoclinic, space group $P2_1/c$ (No. 14), $Z = 8$, $a = 14.986(2)$ Å, $b = 13.396(2)$ Å, $c = 16.351(2)$ Å, $\beta = 108.12(1)^\circ$. The gas phase structures of E_8^{2+} and neutral E_8 ($E = S, Se$) were examined by ab initio methods (B3PW91, MPW1PW91) leading to $\Delta_f H^\circ[S_8^{2+}, g] = 2151$ kJ/mol and $\Delta_f H^\circ[Se_8^{2+}, g] = 2071$ kJ/mol. The observed solid state structures of S_8^{2+} and Se_8^{2+} with the unusually long transannular bonds of 2.8–2.9 Å were reproduced computationally for the first time, and the E_8^{2+} dications were shown to be unstable toward all stoichiometrically possible dissociation products E_n^+ and/or E_4^{2+} [$n = 2-7$, exothermic by 21–207 kJ/mol ($E = S$), 6–151 kJ/mol ($E = Se$)]. Lattice potential energies of the hexafluoroarsenate salts of the latter cations were estimated showing that $S_8(AsF_6)_2$ [$Se_8(AsF_6)_2$] is *lattice stabilized* in the solid state relative to the corresponding AsF_6^- salts of the stoichiometrically possible dissociation products by at least 116 [204] kJ/mol. The fluoride ion affinity of $AsF_5(g)$ was calculated to be 430.5 ± 5.5 kJ/mol [average B3PW91 and MPW1PW91 with the 6-311+G(3df) basis set]. The experimental and calculated FT-Raman spectra of $E_8(AsF_6)_2$ are in good agreement and show the presence of a cross ring vibration with an experimental (calculated, scaled) stretching frequency of 282 (292) cm^{-1} for S_8^{2+} and 130 (133) cm^{-1} for Se_8^{2+} . An atoms in molecules analysis (AIM) of E_8^{2+} ($E = S, Se$) gave eight bond critical points between ring atoms and a ninth transannular (E3–E7) bond critical point, as well as three ring and one cage critical points. The cage bonding was supported by a natural bond orbital (NBO) analysis which showed, in addition to the E_8 σ -bonded framework, weak π bonding around the ring as well as numerous other weak interactions, the strongest of which is the weak transannular E3–E7 [2.86 Å (S_8^{2+}), 2.91 Å (Se_8^{2+})] bond. The positive charge is delocalized over all atoms, decreasing the Coulombic repulsion between positively charged atoms relative to that in the less stable S_8 -like *exo-exo* E_8^{2+} isomer. The overall geometry was accounted for by the Wade–Mingos rules, further supporting the case for cage bonding. The bonding in Te_8^{2+} is similar, but with a stronger transannular E3–E7 ($E = Te$) bonding. The bonding in E_8^{2+} ($E = S, Se, Te$) can also be understood in terms of a σ -bonded E_8 framework with additional bonding and charge delocalization occurring by a combination of transannular $n\pi^*-n\pi^*$ ($n = 3, 4, 5$), and $np^2 \rightarrow n\sigma^*$ bonding. The classically bonded S_8^{2+} (Se_8^{2+}) dication containing a short transannular S^+-S^+ (Se^+-Se^+) bond of 2.20 (2.57) Å is 29 (6) kJ/mol higher in energy than the observed structure in which the positive charge is delocalized over all eight chalcogen atoms.

Introduction

The elucidation of the nature of the blue species observed upon addition of oleum and other oxidizing agents to elemental sulfur has been a challenge to numerous investigators^{1–7} since

* To whom correspondence should be addressed: X-ray crystallography (T.S.C.); thermodynamics (H.D.B.J.); theoretical calculations and Wade–Mingos treatment (I.K.); problem conception, interpretation, and chemistry (J.P.).

[†] Part of this work has been presented at the 1998 CIC Conference in Whistler, BC, Canada, and at the ACS 14th Winter Fluorine Chemistry Conference (1999) in St. Petersburg, FL (Abstract 24).

[‡] Dalhousie University.

[§] University of Warwick.

^{||} University of New Brunswick.

[⊥] University of Karlsruhe.

(1) Weber, R. *J. Prakt. Chem.* **1882**, 133, 218.

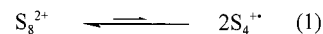
(2) Masson, I.; Argument, C. *J. Chem. Soc.* **1938**, 1705.

(3) Nickless, G. *Inorganic Sulphur Chemistry*; Elsevier: London, 1968; p 412.

(4) Auerbach, R. *Z. Phys. Chem. (Leipzig)* **1926**, 121, 337.

(5) McNeil, D. A. C.; Murray, M.; Symons, M. C. R. *J. Chem. Soc. A* **1967**, 1019.

it was first observed⁸ by Bucholz in 1804. In 1969 one of us (J.P.) prepared^{9,10} the first pure salt of a sulfur homopolyatomic cation, the very *blue* crystalline and essentially diamagnetic $S_8(AsF_6)_2$. In 1971 the salt was shown to contain (X-ray) the discrete S_8^{2+} cation,¹¹ proposed to be in equilibrium with S_4^+ in solution:



In 1976 Low and Beaudet¹² convincingly identified the radical

(6) Burford, N.; Passmore, J.; Sanders, J. C. P. In *From Atoms to Polymers: Isoelectronic Analogies*; Liebman, J. F., Greenberg, A., Eds; VCH: Weinheim, 1989; pp 53–108 and references therein.

(7) Gillespie, R. J.; Passmore, J. *Adv. Inorg. Radiochem.* **1975**, 17, 49 and references therein.

(8) Bucholz, C. F. *Gehlen's Neues J. Chem.* **1804**, 3, 7.

(9) Gillespie, R. J.; Passmore, J. *J. Chem. Soc., Chem. Commun.* **1969**, 1333.

(10) Gillespie, R. J.; Passmore, J.; Ummat, P. K.; Vaidya, O. C. *Inorg. Chem.* **1971**, 10, 1327.

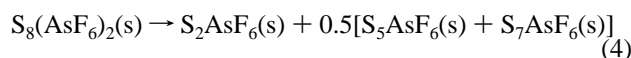
cation in solution as S_5^+ and associated it with the blue color, supported by the work of Burns, Gillespie, and Sawyer¹³ who concluded that S_8^{2+} itself may not be blue. The presence of the lower oxidized S_5^+ sulfur cation implied that in solution S_8^{2+} was in equilibrium with a higher oxidized species, in agreement with the equilibrium



However, it was rather puzzling that there was no evidence for S_3^+ . In 1994 the sums of the first and second ionization energies of S_8 were calculated by ab initio methods by F. Grein.¹⁴ The transannular S–S bond lengths were calculated to be 2.31 Å (HF/3-21G*) and 2.06 Å (HF/6-31G*), respectively,¹⁴ very different from those observed at 2.84 Å,¹¹ but it was assumed that the calculated energies were only slightly different from the true combined ionization potential of S_8 . It was then concluded that S_8^{2+} was unstable in the gas phase with respect to various combinations of monocations, the most exothermic of which was^{15,18}



The standard enthalpy of formation of crystalline $\text{S}_8(\text{AsF}_6)_2$ was determined by fluorine bomb calorimetry and by estimating $\Delta_f H^\ominus$ of the solid S_nAsF_6 salts, it was shown that $\text{S}_8(\text{AsF}_6)_2$ was more stable in the solid state by +172 kJ/mol with respect to the products shown in eq 4.¹⁸ Therefore S_8^{2+} is *lattice*



stabilized in the solid state, and the energetics are consistent with the presence of S_5^+ and S_7^+ in solution. The presence of S_5^+ in solution is well established,¹² and there is some ESR evidence for S_7^+ ^{13,19} and S_2^+ is ESR silent or may dimerize to S_4^{2+} . However, there remained the question of the reliability of the calculated heat of formation of $\text{S}_8^{2+}(\text{g})$. We provided strong evidence^{20,21} to support an earlier conclusion²² that the reported experimental first ionization energy of $\text{S}_4(\text{g})$ and the gaseous standard enthalpy of formation of S_4^+ were substantially

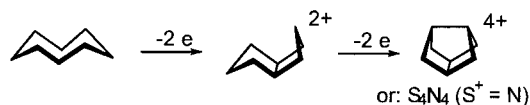
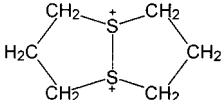
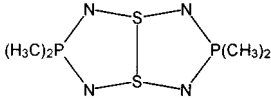


Figure 1. Structural relationships between S_8 , S_8^{2+} , and S_4N_4 .

Table 1. Single S–S Bond Lengths Found in Typical Compounds

compound	$d(\text{S}-\text{S})$ (Å)	ref
FS–SF	1.888(2)	30
HS–SH	2.055(2)	31
S_8	2.060(2)	28
S_8O	2.00–2.20	32
S_7	1.995(3)–2.182(3)	33
	2.124	34
$\text{O}_3\text{S}-\text{SO}_3^{2-}$	2.14–2.15	35–36
$\text{F}_5\text{S}-\text{SF}_5$	2.21(3)	37
$\text{O}_2\text{S}-\text{SO}_2^{2-}$	2.393(2)	38
	2.55	39
S_4N_4	2.58(1)	28

in error (by 159 kJ/mol). This suggests that S_8^{2+} may not dissociate in the gas phase (and in solution) according to eq 3 but by some alternative.

The nature of the bonding in S_8^{2+} has been an unsolved problem since the structure was first elucidated.¹¹ The overall geometry of S_8^{2+} ¹¹ (and the isostructural Se_8^{2+})^{23–26} was not entirely unexpected, being intermediate between those of crown S_8 and the cage-like S_4N_4 (isoelectronic to S_8^{4+} , see Figure 1).^{27–29} However, the cross ring bond lengths of about 2.85(5) Å were shorter than the sum of the sulfur (selenium) van der Waals radii (3.70 and 3.90 Å, respectively) although much longer than a single E–E bond (E = S, 2.05 Å; E = Se, 2.35 Å).²⁸ In fact, a similar situation arises in E_4N_4 , which also has very long S–S (Se–Se) bonds of 2.58 Å (2.73 Å)²⁸ and has also presented a challenge to theory.^{27,28} Moreover, many S–S bonds that to the first order of approximation appear to be single bonds varied considerably in bond length; some examples of these are given in Table 1. Initially¹¹ the bonding was described by the valence bond structures **1**, **2**, and **3** that served to delocalize the positive charge (see Figure 2). Further light was

- (11) Davies, C. G.; Gillespie, R. J.; Park, J. J.; Passmore, J. *Inorg. Chem.* **1971**, *10*, 2781.
 (12) Low, H. S.; Beaudet, R. A. *J. Am. Chem. Soc.* **1976**, *98*, 3849.
 (13) Burns, R. C.; Gillespie, R. J.; Sawyer, J. F. *Inorg. Chem.* **1980**, *19*, 1423.
 (14) $\Delta_f H^\ominus[\text{S}_8^{2+}, \text{g}] = 2301$ kJ/mol at the HF/3-21G* and HF/6-31G* levels of theory. Grein, F.; Sannigrahi, M. Unpublished results, University of New Brunswick.
 (15) The enthalpy of eq 3 was calculated using the standard enthalpies of formation of the gas phase sulfur monocations^{16,17} and the calculated heat of formation of $\text{S}_8^{2+}(\text{g})$.¹⁴
 (16) Wagman, D. D.; Evans, W. H.; Parker, V. B.; Schumm, R. H.; Halow, I.; Bailey, S. M.; Churney, K. L.; Nuttal, R. L. *J. Phys. Chem. Ref. Data* **1982**, *11*, Suppl. 2.
 (17) Lias, S. G.; Bartmess, J. E.; Liebman, J. F.; Holmes, J. L.; Levin, R. D.; Mallard, W. G. *J. Phys. Chem. Ref. Data* **1988**, *17*, Suppl. 1.
 (18) Thomaskiewicz, I.; Passmore, J.; Schatte, G.; Sutherland, G. W.; O'Hare, P. A. G. *J. Chem. Thermodyn.* **1994**, *26*, 299.
 (19) Passmore, J.; Sutherland, G.; Taylor, P.; Whidden, T. K.; White, P. S. *Inorg. Chem.* **1981**, *20*, 3839.
 (20) In an investigation of the mixed open- and closed-shell calculation of the gas phase dimerization energy of 2S_2^+ giving S_4^{2+} , the B3PW91/6-311+G(3df)//B3PW91/6-311+G* level (employed for S_8^{2+}) was found to give values as good as a CCSD(T)/cc-pVD5Z calculation. In addition we established the quality of all calculated properties by reproducing the experimentally found heats of formation of the sulfur monocations. Jenkins, H. D. B.; Jitariu, L. C.; Krossing, I.; Passmore, J.; Suontamo, R. *J. Comput. Chem.* **2000**, *21*, 218.
 (21) Krossing, I.; Passmore, J. *Inorg. Chem.* **1999**, *38*, 5203.
 (22) Berkowitz, J.; Lifshitz, C. *J. Chem. Phys.* **1968**, *48*, 4346.

- (23) McMullan, R. K.; Prince, D. J.; Corbett, J. D. *Inorg. Chem.* **1971**, *10*, 1749.
 (24) Brown, I. D.; Crump, D. B.; Gillespie, R. J. *Inorg. Chem.* **1971**, *10*, 2319.
 (25) Cardinal, G.; Gillespie, R. J.; Sawyer, J. F.; Vekris, J. E. *J. Chem. Soc., Dalton Trans.* **1982**, 765.
 (26) Collins, M. J.; Gillespie, R. J.; Sawyer, J. F. *Acta Crystallogr.* **1988**, *C44*, 405.
 (27) Cassoux, P.; Labarre, J.-F.; Glemser, O. *J. Mol. Struct.* **1972**, *13*, 405.
 (28) Studel, R. *Angew. Chem., Int. Ed. Engl.* **1975**, *10*, 655 and references therein.
 (29) Passmore, J.; Klapötke, T. *Acc. Chem. Res.* **1989**, *22*, 234.
 (30) Kuczkowski, R. L. *J. Am. Chem. Soc.* **1964**, *86*, 3617.
 (31) Winnawisser, M.; Haase, J. Z. *Naturforsch.* **1968**, *23a*, 56.
 (32) Studel, R.; Luger, P.; Bradazcek, H.; Rebsch, M. *Angew. Chem., Int. Ed. Engl.* **1973**, *12*, 452.
 (33) Studel, R. *Top. Curr. Chem.* **1982**, *102*, 149.
 (34) Iwasaki, F.; Toyoda, N.; Akaiishi, R.; Fujihara, H.; Furukawa, N. *Bull. Chem. Soc. Jpn.* **1988**, *61*, 2563.
 (35) Berthold, I.; Weiss, A. Z. *Naturforsch.* **1967**, *22a*, 1440.
 (36) Stanly, E. *Acta Crystallogr.* **1956**, *9*, 897.
 (37) Harrey, R. B.; Bauer, S. H. *J. Am. Chem. Soc.* **1953**, *75*, 2840.
 (38) Dunitz, J. D. *Acta Crystallogr.* **1956**, *9*, 579.
 (39) Burford, N.; Chivers, T.; Coddling, P. W.; Oakley, R. T. *Inorg. Chem.* **1982**, *21*, 982 and references therein.

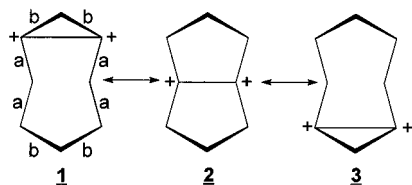


Figure 2. Valence bond structures to account for the transannular bonding in S_8^{2+} .

shed on the problem by the observed similarity of the structure of $Se_2I_4^{2+}$ ^{40,41} and the six central selenium atoms of Se_8^{2+} (isolobal to S_8^{2+} , see Figure 3) leading to the proposal of a six-center intracationic $\pi^*-\pi^*$ bond as an explanation for the observed proximity of the six central chalcogen atoms. This model was supported by CNDO⁴² and also by Hückel⁴³ calculations. The bonding between the two weakly linked SeI_2^+ in $Se_2I_4^{2+}$ was accounted for^{40,41} by assuming that the interaction of the unpaired electrons in each of the SeI_2^+ π^* orbitals (Figure 3) led to dimerization by formation of a six-center-two-electron $\pi^*-\pi^*$ bond (Figure 3). This leads to positive charge delocalization over all six atoms and the formation of one $4p-5p$ π bond delocalized over the four Se–I bonds, i.e., a Se–I bond order of 1.25. Consistently, the experimentally observed Se–I bond lengths were shorter than those in SeI_3^+ with a bond order of 1. This π and $\pi^*-\pi^*$ bonded situation is formed in preference to the classical, all- σ -bonded structure of the isoelectronic As_2I_4 and implies that a similar $\pi^*-\pi^*$ bonding is found in both, Se_8^{2+} and S_8^{2+} , favored over an all- σ -bonded structure having a short transannular S–S bond of about 2.10 Å [cf. $d(S-S) = 2.124$ Å in 1,5-disulfoniabicyclo[3.3.0]octane,³⁴ which is classically bonded]. The model also implies a delocalized $p_\pi-p_\pi$ bond over the four S–S and Se–Se bonds adjacent to the central transannular interaction in S_8^{2+} and Se_8^{2+} . However the 1971 X-ray crystal structure of $S_8(AsF_6)_2$ ¹¹ and a later 1989 structure of $S_8(Sb_3F_{14})(SbF_6)$ ⁴⁴ showed the four central S–S distances (a , in Figure 2) not to be significantly different from the two S–S distances (b , in Figure 2) (see Table 3, a corresponds to S2–S3, S3–S4, S7–S6, S8–S7, and b to S1–S2, S4–S5, S6–S5, S1–S8).

Clearly the bonding situation in S_8^{2+} (and Se_8^{2+}) was not yet resolved. To solve the problem, a precisely determined X-ray crystal structure of $S_8(AsF_6)_2$ was needed as well as a successful modeling of the geometry of $S_8^{2+}(g)$ by ab initio calculations. In addition, the solution of the bonding problem in S_8^{2+} (Se_8^{2+}) would shed light on the nature of the bonding in the other homopolyatomic cations of groups 16 and 17 and the halopoly-chalcogen cations that have nonclassical structures,^{7,45,46} as well as in related molecules containing long $E\cdots E$ bonds (e.g., in Table 1).

In an attempt to prepare $S_{10}(AsF_6)_2$, good crystals of $S_8(AsF_6)_2$ that were not very blue but red in transmitted light were obtained. The synthesis and the X-ray crystal structure determination of this salt as well as the FT-Raman spectra of E_8-

$(AsF_6)_2$ ($E = S, Se$) are reported below for the first time. The ab initio calculations of E_8^{2+} ($E = S, Se$) have proved to be a challenge to theoreticians. Earlier MNDO calculations led to a bicyclic geometry with a transannular S–S bond length of 2.06 Å,⁴⁷ in strong disagreement with the experimental finding. In 1997 Cioslowski et al.⁴⁸ published a paper entitled “Transannular Interactions in S_8^{2+} and Se_8^{2+} : Reality or Artifact?” where various levels of theory (HF/6-311G*, MP2/6-311G*, and BLYP/6-311G*) produced either a shorter transannular bond (2.22 Å, HF) or a longer (or no) transannular bond (3.33 Å, MP2; 3.13 Å, BLYP). As far as we are aware, there is no report of a successful calculation of these species in the literature. However, we have shown^{20,21} that the hybrid HF/DFT method Becke3PerdewWang91 (B3PW91) accurately determines the geometries and dimerization energies of $2E_2^+(g)$ to $E_4^+(g)$ ($E = S, Se$) whereas other methods, although giving correct geometries, provide very poor dimerization energies. We therefore undertook a theoretical study of the geometries, energetics, and vibrational spectra of the E_8^{2+} ($E = S, Se$) dications using the B3PW91 and the new, improved MPW1PW91 levels of theory, the results of which are reported below. We have reexamined the energetics of the dissociation of $S_8^{2+}(g)$ and, using our recently developed relationship between lattice enthalpy and ionic volumes,^{49–52} have calculated the solid state thermodynamics of the octasulfur and octaselenium dications.

Experimental Section

General Procedures and Reagents. General techniques are described in ref 53. All reactions were carried out in a jointless, single-piece apparatus consisting of two thick walled round bottom flasks ($V = 25$ mL) linked by a glass tube incorporating a sintered medium-porosity glass frit. One bulb was connected to a reflux condenser separated by a second glass frit. A glass tubing vent for pressure compensation to the upper end of the condenser was included (in the following referred to as “the apparatus”). One bulb and the condenser of the apparatus were fitted with J. Young or Rotoflo valves. Moisture-sensitive materials, crystals suitable for X-ray crystal structure determination, and all solid products were manipulated as previously described.⁵⁴ FT-Raman spectra were obtained at 150 K from neat samples sealed under nitrogen in 5 mm glass tubes using a Bruker IFS 66 FT-IR spectrometer equipped with a Bruker FRA 106 FT-Raman accessory. In situ NMR samples were prepared in 10 mm thick walled NMR tubes fitted with J. Young valves. NMR spectra were obtained on a variable-temperature, multinuclear Varian 400 MHz spectrometer. ¹⁹F NMR spectra were referenced against external $FCCl_3$ as a standard.

Sulfur (Fisher Scientific, precipitated) and AsF_5 (Ozark-Mahoning) were used as received. SO_2 and SO_2ClF (Matheson) were vacuum distilled onto and stored over CaH_2 and molecular sieves (4 Å), respectively, at least 24 h prior to use. Blue $S_8(AsF_6)_2$ ^{18,55} and green $Se_8(AsF_6)_2$ ⁵⁶ were prepared as previously described.

Attempted Preparation of $S_{10}(AsF_6)_2$ Leading to Red Single Crystals of $S_8(AsF_6)_2$. In one reaction, a 2:1 (by weight) mixture of

- (40) Passmore, J.; Sutherland, G.; Whidden, T.; White, P. S.; Wong, C.-M. *J. Chem. Soc., Chem. Commun.* **1982**, 1098.
 (41) Nandana, W. A. S.; Passmore, J.; White, P. S.; Wong, C.-M. *Inorg. Chem.* **1990**, *29*, 3529.
 (42) Tanaka, K.; Yamabe, T.; Teramae, H.; Fukui, K. *Nouv. J. Chim.* **1979**, *3*, 379.
 (43) Burford, N.; Passmore, J. Unpublished results reported in ref 6.
 (44) Faggiano, R.; Gillespie, R. J.; Sawyer, J. F.; Vekris, J. E. *Acta Crystallogr.* **1989**, *C45*, 1847.
 (45) Passmore, J. In *Studies in Inorganic Chemistry*; Stuedel, R., Ed.; Elsevier: New York, 1992; Vol. 14, Chapter 19, pp 373–406.
 (46) Brownridge, S.; Krossing, I.; Passmore, J.; Jenkins, H. D. B.; Roobottom, H. K. *Coord. Chem. Rev.* **2000**, *197*, 397.

- (47) Baird, N. C. *J. Comput. Chem.* **1984**, *5*, 35.
 (48) Cioslowski, J.; Gao, X. *Int. J. Quantum Chem.* **1997**, *65*, 609.
 (49) Jenkins, H. D. B.; Passmore, J.; Roobottom, H. K.; Glasser, L. *Inorg. Chem.* **1999**, *38*, 3609.
 (50) Roobottom, H. K.; Jenkins, H. D. B.; Passmore, J.; Glasser, L. *J. Chem. Educ.* **1999**, *76*, 1570.
 (51) Mallouk, T. E.; Rosenthal, G. L.; Muller, G.; Brusasco, R.; Bartlett, N. *Inorg. Chem.* **1984**, *23*, 3167.
 (52) Jenkins, H. D. B.; Roobottom, H. K.; Passmore, J. *Inorg. Chem.*, submitted for publication.
 (53) Murchie, M. P.; Kapoor, R.; Passmore, J.; Schatte, G. *Inorg. Synth.* **1996**, *31*, 80.
 (54) Brownridge, S.; Cameron, T. S.; Passmore, J.; Schatte, G.; Way, T. *J. Chem. Soc., Dalton Trans.* **1996**, 2553 and references therein.
 (55) Murchie, M. P.; Passmore, J. *Inorg. Synth.* **1986**, *24*, 76.
 (56) Nandana, W. A. S.; Passmore, J.; White, P. S.; Wong, C. M. *Inorg. Chem.* **1989**, *28*, 3320.

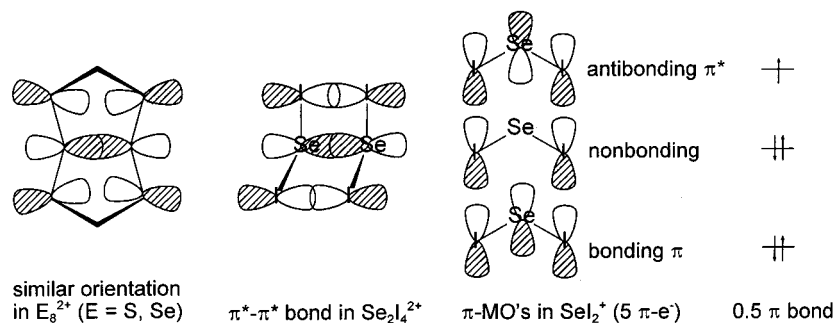


Figure 3. Six-center intracationic $\pi^*-\pi^*$ bond in $Se_2I_4^{2+}$ and E_8^{2+} ($E = S, Se$).

SO_2 and SO_2ClF was refluxed in the apparatus with 1.00 g (1.58 mmol) of blue $S_8(AsF_6)_2$ placed on the frit and 0.10 g (0.39 mmol) of S_8 in the bulb below. The blue $S_8(AsF_6)_2$ dissolved slowly in the solvent, which condensed onto the sides of the condenser, on cooling with cold flowing water, and washed down onto the sulfur-containing bulb. The color changed immediately to a brownish red solution over a brownish red precipitate. After this mixture was refluxed for 2 days without stirring, large red crystals were formed, and they were identified as $S_8(AsF_6)_2$ by X-ray crystallography (see below). Attempts to repeat this reaction were unsuccessful and typically gave crystals that were red in transmitted light and blue in reflected light when examined under the microscope. These latter crystals were shown by X-ray diffraction to be identical to those above. A similar but not identical reaction [0.11 g of S_8 , 0.43 mmol; 1.08 g of $S_8(AsF_6)_2$, 1.70 mmol] in SO_2 (6.90 g) gave an intensely brown-red solution at room temperature within 2 min. After 5 days of refluxing, all of the $S_8(AsF_6)_2$ had dissolved, giving a dark blue solution over a dark blue precipitate. Upon addition of SO_2ClF (6.14 g) a dark red-brown solution was formed over a precipitate of the same color. The solvent was slowly condensed into the second bulb (5 days) and finally removed in vacuo. The bulk, dark red-brown material was examined under the microscope and showed the presence of dark red crystals and dark red, orange, and yellow (probably S_8) crystalline material. The FT-Raman spectrum of the bulk material was identical to that of elemental sulfur (which gives a very intense Raman spectrum). Numerous attempts to prepare $S_{10}(AsF_6)_2$ by the direct oxidation of elemental sulfur by arsenic pentafluoride in a 2:1 (mole ratio) $SO_2:SO_2ClF$ mixture in a two-bulbed vessel led to a red amorphous material containing some dark brown crystals that poorly diffracted X-rays. In order to determine whether SO_2ClF reacted with $S_8(AsF_6)_2$, an in situ ^{19}F NMR experiment was conducted in which $S_8(AsF_6)_2$ was prepared in a 2:1 (mole ratio) mixture of SO_2 (2.03 g, 31.7 mmol) and SO_2ClF (1.95 g, 16.5 mmol) from 0.15 g of S_8 (0.58 mmol) and 0.44 g of AsF_5 (2.61 mmol). This red solution above an undissolved red/blue solid was kept at room temperature, and the ^{19}F NMR spectrum was recorded at -70 °C after 1 day and after 2 and 4 weeks. These spectra only showed peaks attributable to SO_2ClF (δ $^{19}F = 98.6$ ppm), a trace amount of OSF_2 (δ $^{19}F = 72.2$ ppm) (2% and 3% with respect to SO_2ClF after 2 and 4 weeks),⁵⁷ and an average signal for AsF_3 , AsF_6^- , and AsF_5 (δ ^{19}F (room temperature) = -46.8 ppm). We conclude that $S_8(AsF_6)_2$ is relatively stable in $SO_2ClF:SO_2$ mixtures over 2–4 weeks.

X-ray Crystal Structure Determination. A dark red block crystal of $F_{12}S_8As_2$ (0.30 × 0.20 × 0.50 mm) was mounted on a glass fiber. All measurements were made on an AFC5R diffractometer with graphite-monochromated Mo $K\alpha$ radiation and a rotating anode generator (50 kV, 160 mA). Cell constants and an orientation matrix for data collection were obtained from a least-squares refinement using the setting angles of 24 carefully centered reflections in the range $35.03^\circ < 2\theta < 42.07^\circ$. Data were collected at 213 ± 1 K using the $\omega-2\theta$ scan mode ($2\theta_{max} = 46^\circ$).⁵⁸ Of the 4841 reflections recorded, 4571 were unique ($R_{int} = 0.022$). No decay correction was applied. $\mu(Mo K\alpha)$ is 54.7 cm^{-1} . An empirical absorption correction based on azimuthal scans of several reflections was applied which resulted in a

Table 2. Crystallographic Data for $S_8(AsF_6)_2$

chem formula	$F_{12}S_8As_2$	$V, \text{\AA}^3$	3119.7(8)
fw	634.30	Z	8
cryst syst	monoclinic	temp, K	213
space group	$P2_1/c$ (No. 14)	$\lambda, \text{\AA}$	0.71069
$a, \text{\AA}$	14.986(2)	$\rho_{calcd}, g\ cm^{-3}$	2.701
$b, \text{\AA}$	13.396(2)	μ, cm^{-1}	54.66
$c, \text{\AA}$	16.351(2)	R^a	0.029
β, deg	108.12(1)	R_w^b	0.030

$$^a R = \sum(|F_o| - |F_c|) / \sum|F_o|. \quad ^b R_w = [\sum w(|F_o| - |F_c|)^2 / \sum (w|F_o|)^2]^{1/2}.$$

transmission factor ranging from 0.69 to 1.00. The data were corrected for Lorentz and polarization effects. The structure was solved by and expanded using standard Fourier techniques.⁵⁹ All atoms were refined anisotropically. The final cycle of full-matrix least-squares refinement on F was based on 2516 observed reflections [$I > 3.00\sigma(I)$] and 397 variable parameters, converged with unweighted and weighted agreement factors of $R = \sum||F_o| - |F_c|| / \sum|F_o| = 0.029$ and $R_w = [\sum w(|F_o| - |F_c|)^2 / \sum wF_o^2]^{1/2} = 0.030$ (GOF = 1.39). The weighting scheme was based on counting statistics and included a factor ($p = 0.010$) to downweight the intense reflections. The maximum and minimum peaks on the final difference Fourier map corresponded to 0.58 and -0.41 $e/\text{\AA}^3$, respectively. All calculations were performed using the TEXSAN⁶⁰ crystallographic software package of Molecular Structure Corporation. Crystallographic data are summarized in Table 2, while more complete details of data collection and refinement are included in the Supporting Information.

The two independent S_8^{2+} cations (A and B, refer to Figure 4) were corrected for librational motion by a TLS analysis {ring A, $R = 0.072$, $R_{ii} = 0.043$, rms = 0.0017; ring B, $R = 0.099$, $R_{ii} = 0.061$, rms = 0.0022; $R, [(\sum(wt.Del(U))^2) / (\sum(wt.U_{obs})^2)]^{-1/2}$; rms of $w_t.del(U), [(\sum(Del(U))^2) / (\sum(wt^2))]^{-1/2}$.

Computational Details

All calculations have been performed using either the Gaussian 94W⁶¹ or the Gaussian 98W⁶² suite of programs. Visualization of the optimized structures and critical points were made using Schwenk's RESVIEW program,⁶³ whereas graphic representations of the calculated molecular orbitals were obtained using either ORBDRAW or CHEM3D Ultra.⁶⁴ Calculated vibrational frequencies have been animated using HyperChem.⁶⁵ Becke's three-parameter exchange functional⁶⁶ combined with the 1991 Perdew Wang correlation functional⁶⁷ (B3PW91) were

(59) The DIRDIF-94 program system: Beurskens, P. T.; Admiraal, G.; Beurskens, G.; Bosman, W. P.; de Gelder, R.; Israel, R.; Smits, J. M. M. Technical Report of the Crystallography Laboratory; University of Nijmegen: The Netherlands, 1994.

(60) TEXSAN for Windows version 1.05: Single-Crystal Structure Analysis Package, Molecular Structure Corporation: The Woodlands, TX, 1997–1998.

(61) Performed with the program Gaussian 94, Revision E.3: Frisch, M. J.; Trucks, G. W.; Schlegel, H. B.; Gill, P. M. W.; Johnson, B. G.; Robb, M. A.; Cheeseman, J. R.; Keith T.; Petersson, G. A.; Montgomery, J. A.; Raghavachari, K.; Al-Laham, M. A.; Zakrzewski, V. G.; Ortiz, J. V.; Foresman, J. B.; Peng, C. Y.; Ayala, P. Y.; Chen, W.; Wong, M. W.; Andres, J. L.; Replogle, E. S.; Gomperts, R.; Martin, R. L.; Fox, D. J.; Binkley, J. S.; Defrees, D. J.; Baker, J.; Stewart, J. P.; Head-Gordon, M.; Gonzalez, C.; Pople, J. A. Gaussian, Inc.: Pittsburgh, PA, 1995.

(57) OSF_2 may arise from reaction of $S_8(AsF_6)_2$ with traces of moisture.

(58) The geometry of the cooling system precludes data collection at a higher angle.

employed for the accurate description^{20,21} of homopolyatomic sulfur and selenium cations, and this approach was selected to compute the properties of neutral S_8 and the endo-exo S_8^{2+} . At the hybrid HF/DFT level of theory, the 1996 by Vizenzo and Barone modified PW exchange functional combined with the 1991 PW correlation functional⁶⁷ (=MPW1PW91) gave the best results for related homopolyatomic sulfur species, as was found in an investigation of the geometries and energetics of S_2 , S_2^+ , and S_4^{2+} .⁶⁸ Full optimizations (including frequency analysis) have been performed using the 6-311+G* basis set (3-21G* for MPW1PW91) to determine stationary points on the hypersurface, followed by a reoptimization with the 6-311G(2df) basis set and by single-point calculations using the flexible 6-311+G(3df) basis set to obtain accurate total energies. Zero-point energies (6-311+G* basis set) were included for all thermodynamic calculations and derived enthalpies corrected to 298 K. Natural bond orbital (NBO)⁶⁹ analyses were performed for E_8^{2+} and neutral E_8 , employing B3PW91/6-311+G(3df)//B3PW91/6-311G(2df) ($E = S$) or MPW1PW91/6-311G(2df)//MPW1PW91/3-21G* ($E = Se$). Total electron density differences were computed at the MPW1PW91/3-21G* level of theory with the help of the CUBMAN program included in Gaussian 98W.⁶² Atoms in molecules (AIM) analyses were carried out using the AIMPAC series of programs,^{70–73} with the electron density obtained at the B3PW91/6-311G(2df) ($E = S$) or MPW1PW91/6-311G(2df) ($E = Se$) level of theory. Calculations were also done with the same method using the experimental geometries for S_8^{2+} (this work) and Se_8^{2+} in $(Se_8)(Te_6)(AsF_6)_6(SO_2)$.²⁶ The new AIM2000 program developed by Friedrich Biegler-König et al.⁷⁴ was used to obtain the molecular graphs and help confirm the assignments of the ring critical points.

Results and Discussion

Synthesis of Red $S_8(AsF_6)_2$. Attempts to prepare crystals of $S_{10}(AsF_6)_2$ [cf. $Se_{10}(AsF_6)_2$] by reaction of blue $S_8(AsF_6)_2$ with $^{2/8}S_8$ in a 2:1 SO_2/SO_2ClF mixture proved to be unsuccessful. A single crystal, with a red appearance, obtained from the brown-red product was crystallographically shown to be $S_8(AsF_6)_2$. Other crystals picked from a similar preparation were characterized as $S_8(AsF_6)_2$ (X-ray) and then examined under

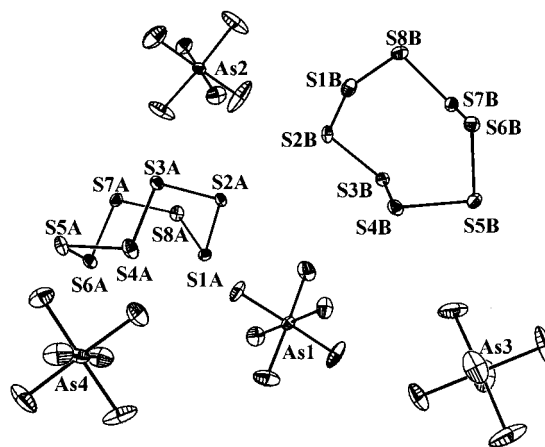
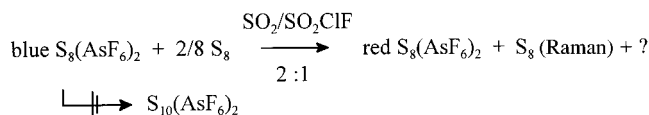


Figure 4. ORTEP plot of the two independent molecules in the asymmetric unit of $S_8(AsF_6)_2$; thermal ellipsoids are drawn at the 25% probability level.

the microscope and found to be red in transmitted but blue in reflected light. The red color observed in reflected light for the one crystal may be due to a surface coating of red material which is likely to be the more soluble $S_{19}(AsF_6)_2$ or a lower oxidized sulfur homopolyatomic cation salt.



It is possible that the reflected color depends on the nature of the surface (blue implying S_5^+ and/or other sulfur radical cations, see below) whereas the red color observed under transmitted light depends on the composition of the crystal as a whole. This is direct evidence that S_8^{2+} is not blue but red, as implied by earlier solution studies.^{6,12,13}

X-ray Crystal Structure of $S_8(AsF_6)_2$. A single-crystal X-ray structure of red monoclinic $S_8(AsF_6)_2$ was determined in the solid state at 213 K. An ORTEP representation of the two independent molecules in the unit cell is depicted in Figure 4. The structural parameters are summarized in Table 3, additionally corrected for librational motion and compared to a previously published structure of S_8^{2+} . The structure contains two unique S_8^{2+} dications (A and B), and each S_8^{2+} dication consists of a folded eight-membered ring of approximate C_3 symmetry having an endo-exo conformation with close transannular contacts, as was found in the original analysis¹¹ and in the later report of S_8^{2+} in $S_8(SbF_6)(Sb_3F_{14})$.⁴⁴ The standard deviations for the S–S bond lengths in the new determination of the hexafluoroarsenate salt improved considerably from 0.01–0.012 Å (1971 structure)¹¹ and 0.005 Å (1989 structure,⁴⁴ not corrected for librational motion) to 0.003 Å (present determination). The small bond alternations observed in the 1971 structure ($a > b$, **1** in Figure 2) are found in the skeletal bonds for three out of four equivalent pairs in the 1989 structure [$S_8(SbF_6)(Sb_3F_{14})$ salt] and for seven out of eight pairs (five of which are significantly different) in the two crystallographically different (A and B, Figure 4) S_8^{2+} in the present study, with eight pairs being of equal length (see figure in Supporting Information). The differences in the chemically equivalent, but crystallographically different, S–S bond lengths may be attributed to normal crystallographic errors and also from differing $S \cdots F$ contacts. We conclude that the slight alternation in bond length has been established. The transannular bonds in the two crystallographically different S_8^{2+} vary by more than 3σ [S2–

- (62) Performed with the program Gaussian 98, Revision A.3: Frisch, M. J.; Trucks, G. W.; Schlegel, H. B.; Scuseria, G. E.; Robb, M. A.; Cheeseman, J. R.; Zakrzewski, V. G.; Montgomery, J. A.; Stratmann, R. E. Jr.; Burant, J. C.; Dapprich, S.; Millam, J. M.; Daniels, A. D.; Kudin, K. N.; Strain, M. C.; Farkas, O.; Tomasi, J.; Barone, V.; Cossi, M.; Cammi, R.; Mennucci, B.; Pomelli, C.; Adamo, C.; Clifford, S.; Ochterski, J.; Petersson, G. A.; Ayala, P. Y.; Cui, Q.; Morokuma, K.; Malick, D. K.; Rabuck, A. D.; Raghavachari, K.; Foresman, J. B.; Cioslowski, J.; Ortiz, J. V.; Stefanov, B. B.; Liu, G.; Liashenko, A.; Piskorz, P.; Komaromi, I.; Gomperts, R.; Martin, R. L.; Fox, D. J.; Keith, T.; Al-Laham, M. A.; Peng, C. Y.; Nanayakkara, A.; Gonzalez, C.; Challacombe, M.; Gill, P. M. W.; Johnson, B.; Chen, W.; Wong, M. W.; Andres, J. L.; Gonzalez, C.; Head-Gordon, M.; Replogle, E. S.; Pople, J. A. Gaussian, Inc.: Pittsburgh, PA, 1998.
- (63) RESVIEW version 2.21: Schwenk, H., University of Munich, 1998.
- (64) Chem3D Ultra, CambridgeSoft, 1998.
- (65) HyperChem, V.3.0, Autodesk, 1993. Obtaining correct assignments of the vibrations of a homopolyatomic system is difficult since all vibrations are heavily mixed. Best results were obtained by increasing the number of frames to be calculated (50 to 60) and enlarge the amplitude (1.0 Å) in the IR animation of HyperChem.
- (66) Becke, A. D. *J. Chem. Phys.* **1993**, *98*, 5648.
- (67) Perdew, J. P.; Wang, Y. *Phys. Rev.* **1992**, *B45*, 13244.
- (68) E.g., MPW1PW91/6-311+G* gives better results than all other performed hybrid HF/DFT calculations in ref 20.
- (69) Reed, A. E.; Curtiss, L. A.; Weinhold, F. *Chem. Rev.* **1988**, *88*, 899 and references therein.
- (70) Bader, R. F. W. *Acc. Chem. Res.* **1985**, *18*, 9.
- (71) Biegler-König, F. W.; Bader, R. F. W.; Tang, T. H. *J. Comput. Chem.* **1982**, *3*, 317.
- (72) Tang, T. H.; Bader, R. F. W.; MacDougall, P. *Inorg. Chem.* **1985**, *24*, 2047.
- (73) Popelier, P. *Atoms in Molecules, An Introduction*; Prentice Hall: England, 2000; 164 pp and references therein.
- (74) AIM2000—A program to analyze and visualize atoms in molecules: Biegler-König, F. W.; Schönbohm, J.; Bayles, D. Submitted to *J. Comput. Chem.*

Table 3. Comparison of New and Published Structural Parameters of the S_8^{2+} Dication

$d(\text{S}-\text{S})$ (Å)	1989 ^a	this work				av ^c
		# A ^b	# B ^b	# A, corr ^b	# B, corr ^b	
S3-S7	2.906(5)	2.877(3)	2.824(3)	2.886(3)	2.831(3)	2.859
S2-S8	na	2.876(3)	3.003(3)	2.888(3)	3.013(3)	2.956
S4-S6	na	3.031(3)	2.943(3)	3.043(3)	2.953(3)	2.998
S1-S2	2.032(5)	2.037(3)	2.061(3)	2.044(3)	2.057(3)	2.051
S2-S3	2.054(5)	2.021(3)	2.035(3)	2.025(3)	2.057(3)	2.041
S1-S8	2.043(5)	2.047(3)	2.047(3)	2.064(3)	2.069(3)	2.067
S8-S7	2.037(5)	2.027(3)	2.046(3)	2.040(3)	2.037(3)	2.039
S3-S4	2.008(5)	2.038(3)	2.030(3)	2.048(3)	2.043(3)	2.046
S7-S6	2.001(5)	2.040(3)	2.035(3)	2.045(3)	2.042(3)	2.044
S4-S5	2.041(5)	2.050(3)	2.050(3)	2.064(3)	2.063(3)	2.064
S6-S5	2.033(5)	2.045(3)	2.056(3)	2.055(3)	2.052(3)	2.054

bond angles (deg)	1989 ^a	this work				av ^c
		# A ^b	# B ^b	# A, corr ^b	# B, corr ^b	
S1-S2-S3	101.4(2)	103.5(1)	101.8(1)	103.6(1)	101.6(1)	102.6
S2-S3-S4	104.5(2)	104.2(1)	104.3(1)	104.0(1)	104.1(1)	104.1
S3-S4-S5	98.1(2)	98.1(1)	97.5(1)	98.1(1)	97.1(1)	97.6
S4-S5-S6	93.1(2)	95.4(1)	91.8(1)	95.6(1)	91.6(1)	93.6
S5-S6-S7	98.5(2)	97.0(1)	97.8(1)	96.9(1)	97.4(1)	97.2
S6-S7-S8	103.5(2)	104.1(1)	104.2(1)	104.0(1)	104.0(1)	104.0
S7-S8-S1	101.8(2)	101.9(1)	100.4(1)	102.0(1)	100.2(1)	101.1
S8-S1-S2	94.0(2)	89.4(1)	93.8(1)	89.4(1)	94.0(1)	91.7

^a 1989, S_8^{2+} in $\text{S}_8(\text{SbF}_6)(\text{Sb}_3\text{F}_{14})$.⁴⁴ ^b This work, S_8^{2+} in $\text{S}_8(\text{AsF}_6)_2$ at 213 K. # A and # B indicate the two crystallographically independent dications, and “corr” denotes the bond distances and angles corrected for librational motion. ^c Average bond lengths and bond angles corrected for librational motion.

Table 4. Structural Parameters of AsF_6^- and $\text{S}\cdots\text{F}$ Contacts

	$d(\text{As}-\text{F})$ (Å)	contact $\text{S}\cdots\text{F}$ (Å)		$d(\text{As}-\text{F})$ (Å)	contact $\text{S}\cdots\text{F}$ (Å)
As1-F1	1.728(5)	S1A: 2.929 S3B: 3.009	As3-F13	1.672(6)	S1B: 2.833
As1-F2	1.703(5)	S2A: 3.040 S4A: 3.090	As3-F14	1.706(5)	S1A: 3.081 S1B: 3.125
As1-F3	1.718(5)	S2A: 3.151 S6B: 3.154	As3-F15	1.692(5)	
As1-F4	1.699(4)	S6B: 3.019	As3-F16	1.687(5)	S5B: 2.969 S6B: 3.117 S8B: 2.923 S2A: 2.986
As1-F5	1.704(6)	S7B: 2.904 S3B: 3.031 S8B: 3.117	As3-F17	1.711(5)	
As1-F6	1.708(5)	S4B: 2.734 S6A: 3.013	As3-F18	1.691(5)	S8A: 2.922
As2-F7	1.717(5)	S3A: 2.950 S2A: 2.953	As4-F19	1.724(5)	S4A: 3.021 S1A: 3.156
As2-F8	1.685(5)	S7A: 3.018 S3A: 3.117	As4-F20	1.712(5)	
As2-F9	1.704(6)	S4B: 2.945 S5B: 3.030	As4-F21	1.694(5)	S1A: 2.941
As2-F10	1.715(6)	S5A: 3.042	As4-F22	1.716(5)	S3A: 3.045 S7A: 3.069
As2-F11	1.684(6)	S1B: 2.910	As4-F23	1.716(5)	
As2-F12	1.664(6)	S5B: 3.090	As4-F24	1.706(5)	S8A: 3.083

S8, 2.876(3) and 3.003(3) Å; S3-S7, 2.824(3) and 2.877(3) Å; S5-S6, 2.943(3) and 3.031(3) Å]. These weak and easily distorted bonds (see below) are strongly affected by $\text{S}\cdots\text{F}$ contacts, which are different in each case. The average S-S single bond length in the cations is 2.042 Å (uncorrected), 2.051 Å (corrected), shorter than that found in elemental sulfur [$d(\text{S}-\text{S}) = 2.047$ Å (uncorrected), 2.060 Å (corrected)].²⁸ Correcting the distances for librational motion increases the S-S bond lengths by roughly 0.01 Å (see Table 3). Equivalent bond angles in the two cations differ by up to four degrees (esd's: 0.1°). All sulfur atoms exhibit at least one primary sulfur-fluorine contact (2.734–3.042 Å), well below the sum of their van der Waals radii (3.20 Å). The respective atomic charges residing on the sulfur atoms have been estimated employing Brown's

methodology⁷⁵ and are summarized together with the calculated natural charges in Figure 13 and are discussed below.

Structural parameters of the AsF_6^- anions and $\text{S}\cdots\text{F}$ contacts are given in Table 4. The As-F bond lengths range from 1.660(6) to 1.728(5) Å and average to 1.702(5) Å. Twenty-one of the twenty-four fluorine atoms exhibit at least one, and up to three, sulfur contacts shorter than 3.20 Å (2.734–3.156 Å). A similar situation, for example, is found in $\text{S}_4(\text{AsF}_6)_2\cdot\text{AsF}_3$

(75) The contacts S (in valency units v.u.) have been defined as $S = (R/R_0)^N$, where R is the observed distance, R_0 is the covalent bond distance (bond order = 1) of the bond in question, and N is an empirically derived constant. For $\text{S}\cdots\text{F}$, $N = 3.8$ and $R_0 = 1.64$ Å. Brown, I. D. In *Structure and Bonding in Crystals*; O'Keefe, M., Navrotsky, A., Eds.; Academic Press: London, 1981; Vol. 2, 1.

and $S_4(AsF_6)_2 \cdot 0.6SO_2$.^{76–82} The shorter $S \cdots F$ contacts (2.664–2.763 Å) in the latter species are due to the increased charge residing on each sulfur atom (+0.5 in S_4^{2+} vs +0.2 to +0.3 in S_8^{2+} , see below). $F-As-F$ bond angles of the AsF_6^- anions in $S_8(AsF_6)_2$ deviate less than 2° from orthogonality, indicating nearly undistorted octahedra. The sums of the $F \cdots S$ valency units per AsF_6^- are 0.58 ($As_4F_6^-$), 0.84 ($As_3F_6^-$), 0.93 ($As_2F_6^-$), and 1.23 ($As_1F_6^-$) (total 3.58, expected 4.0),⁷¹ indicating that it is preferable to average the calculated charges residing on the sulfur atoms (see below). A view of the unit cell along the monoclinic axis is included in the Supporting Information.

Ab Initio Computation of Neutral E_8 and E_8^{2+}

The unusual bonding observed in the E_8^{2+} ($E = S, Se$) dication, has been a goal for a number of theoretical investigations since 1979.^{14,42,43,47,48} Se_8^{2+} has received less computational attention, having a large number (270) of electrons compared to 126 in S_8^{2+} . It also has low symmetry (C_s) and therefore is demanding in CPU time. Similar difficulties are encountered as for S_8^{2+} .^{42,43,48}

Calculated Geometries of S_8 and S_8^{2+} . A preliminary optimization of S_8^{2+} was done by one of us (R.J.D.) utilizing pure DFT and the Becke88Perdew86 (B88P86) level of theory in conjunction with a double- ζ basis set augmented with one set of polarizing d and f functions. Although the geometry obtained mirrored the transannular S_3-S_7 distance, the calculated bond length alternation within the ring did not fit the observed situation,⁸³ and consequently we continued utilizing the more sophisticated hybrid HF-DFT levels of theory. Employing the B3PW91 level of theory and the 6-311+G* and the 6-311G(2df) basis sets, we fully optimized the structures of neutral S_8 (D_{4d}) and exo–endo S_8^{2+} (C_s). The calculated and experimental bond distances and angles for S_8 [exptl, 2.060(2) Å, 108.0°; 6-311+G*, 2.088 Å, 109.2°; 6-311G(2df), 2.060 Å, 108.4°] and S_8^{2+} have been deposited. The calculated and experimental structure of S_8^{2+} is depicted in Figure 5. Computed and experimental geometries of neutral S_8 and the dication S_8^{2+} are in excellent agreement, especially for the structures optimized with the large 6-311G(2df) basis set. Using this geometry, calculated and experimental bond lengths in the eight-membered ring agree almost to within the standard deviation of the experimental data (0.003 Å). In the smaller 6-311+G* basis set, all distances are consistently overestimated by 1.7–1.8%, as was found earlier^{20,21} for S_4^{2+} . A small but definite longer–shorter–shorter–longer bond alternation is found in both of the optimized geometries, in agreement with the experimental values. The maximum deviations of the calculated bond angles from the averaged experimental values are +2.3° [6-311G(2df)]

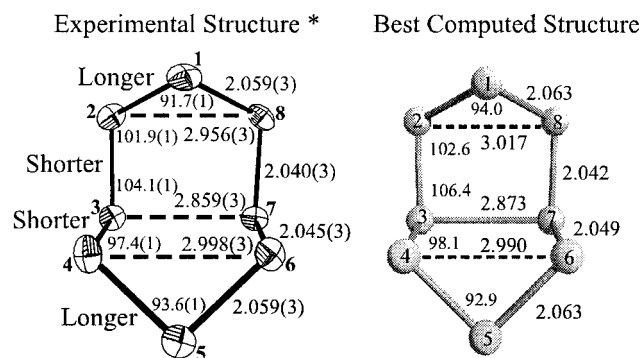


Figure 5. Comparison of the averaged experimental (local C_s symmetry, this work) and the best computed structure for the S_8^{2+} dication [B3PW91/6-311G(2df)]. (*) The designated standard deviations are those observed for the individual bond lengths (Å) and angles (deg).

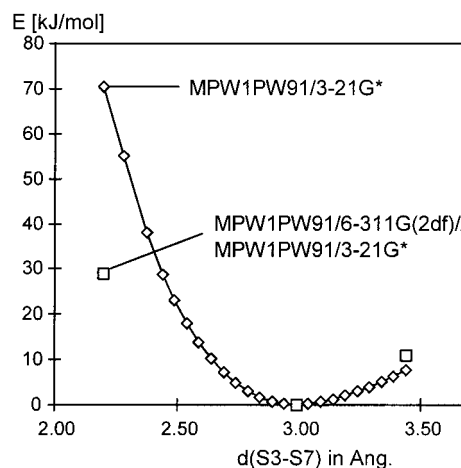


Figure 6. Relaxed potential energy scan of the transannular S_3-S_7 bond in S_8^{2+} (MPW1PW91/3-21G*).

and +3.8° [6-311+G*], a range within which also the two crystallographically independent S_8^{2+} cations differ (see above). The shorter transannular interactions of 2.873–3.017 Å, calculated with the larger basis set, are well within the experimental range (2.831–3.043 Å). Differences exist in the experimental and computed S_2-S_8 and S_4-S_6 transannular distances, which are attributed to the differences in $S \cdots F$ contacts (see X-ray crystal structure discussion). The average $S-S$ bond lengths of S_8^{2+} are calculated to be 2.054 and 2.085 Å, respectively, shorter than those calculated for neutral S_8 at the respective levels (by 0.006 and 0.003 Å; exptl, 0.009 Å), which indicates the presence of additional $S-S$ bonding in S_8^{2+} . Adopting the new MPW1PW91 level to investigate this system further, the 3-21G* basis set is sufficient to describe the geometry of S_8^{2+} adequately and reproduces the experimentally observed longer–shorter–shorter–longer bond alternation (see Figure 5) better than the B3PW91 level with the larger 6-311+G* basis set, highlighting the need to include an accurate description of electron correlation when modeling this species.

We performed a relaxed potential energy scan of the transannular S_3-S_7 bond in the range between 2.20 and 3.44 Å using MPW1PW91/3-21G* and all the parameters left unrestrained, whereupon S_8^{2+} is found within a shallow potential well. The results are shown in Figure 6. To analyze the changes in the bonding in S_8^{2+} when going from the classically bonded structure,⁸⁴ with a short S_3-S_7 distance of 2.20 Å, to the open system at $d(S_3-S_7) = 3.44$ Å, we performed NBO analyses of both these geometries employing the MPW1PW91/6-311G(2df) electron density.⁸⁵ Structural parameters, NBO charges, and

(76) Passmore, J.; Sutherland, G. W.; White, P. S. *J. Chem. Soc., Chem. Commun.* **1980**, 330.

(77) Passmore, J.; Sutherland, G. W.; White, P. S. *Inorg. Chem.* **1982**, *21*, 2717.

(78) Passmore, J.; Sutherland, G. W.; Widden, T. K.; White, P. S.; Wong, C. H. *Can. J. Chem.* **1985**, *63*, 1209.

(79) Dionne, I. M.Sc. Thesis, University of New Brunswick, 1993.

(80) Faggiani, R.; Gillespie, R. J.; Sawyer, J. F.; Vekris, J. E. *Acta Crystallogr.* **1989**, *C45*, 1847.

(81) Murchie, M. P.; Passmore, J.; Sutherland, G. W.; Kapoor, R. *J. Chem. Soc., Dalton. Trans.* **1992**, 503.

(82) Cameron, T. S.; Dionne, I.; Jenkins, H. D. B.; Parsons, S.; Passmore, J.; Roobottom, H. K. *Inorg. Chem.* **2000**, *39*, 2042.

(83) Optimization proceeded in C_1 symmetry, and the minimum has no imaginary frequencies. S_1-S_2 2.072; S_2-S_3 2.071; S_3-S_4 2.062; S_4-S_5 2.077; S_5-S_6 2.075; S_6-S_7 2.066; S_7-S_8 2.071; S_8-S_1 2.067; S_2-S_8 3.005; S_3-S_7 2.881; S_4-S_6 3.001; bond angles range from 92.6° to 104.7°, Hirshfeld charges from 0.178 (S_1) to 0.287 ($S_{3,7}$).

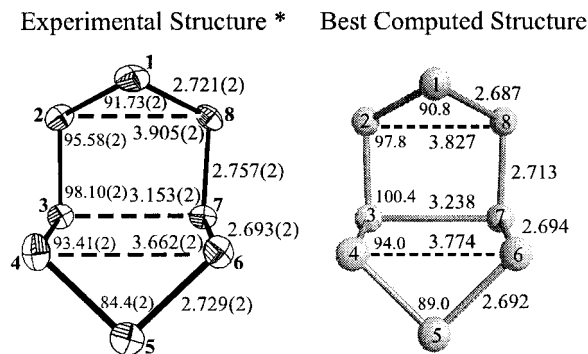


Figure 9. Comparison of the averaged experimental [local C_s symmetry, in $\text{Te}_8(\text{ReCl}_6)$] and the computed structure for the Te_8^{2+} dication [B88P86/Dz(d, f)]. (*) The designated standard deviations are those observed for the individual bond lengths (Å) and angles (deg).

in Se_8^{2+} when compared to that found in S_8^{2+} (see Figure 6). Increasing the Se3–Se7 distance from 2.776 Å at the minimum by 0.9 Å to 3.67 Å changes the total energy by only 6.62 kJ/mol.⁸⁸ For shorter transannular bonds, corresponding to a classical picture⁸⁹ with higher localized charges on the Se3 and Se7 atoms, the total energy rises only by 5.70 kJ/mol [$d(\text{Se}–\text{Se}) = 2.57$ Å], considerably less than in the sulfur case (70 kJ/mol at the same level).

Calculated Geometries of Te_8 and Te_8^{2+} . Five solid state structures of salts containing the Te_8^{2+} dication are known to date.^{87,90–92} Only two of these contain a Te_8^{2+} dication isostructural to the E_8^{2+} geometries described above: found in $\text{Te}_8(\text{ReCl}_6)$ ⁹⁰ and in $\text{Te}_8(\text{HfCl}_6)$.⁸⁷ Te_8 (D_{4d}) and Te_8^{2+} (C_s) were optimized by one of us (R.J.D.) utilizing the B88P86/DZ(d,f) level of theory. However, due to the large scale of the calculation, no frequency analyses were performed. The computed Te_8^{2+} geometry matches the experimentally found Te_8^{2+} geometry in $\text{Te}_8(\text{ReCl}_6)$ reasonably well (comparison table has been deposited). The calculated geometry and experimental geometry of Te_8^{2+} in $\text{Te}_8(\text{ReCl}_6)$ are compared in Figure 9. The overall geometry and bond distances of the experimental Te_8^{2+} structure are reproduced by the calculation to within 0.044 Å and 3.6° (in the ring). All calculated Te–Te bond lengths apart from Te3–Te4 are about 0.03–0.04 Å shorter than the experimental values. However, the transannular distances Te2–Te8, Te3–Te7, and Te4–Te6 differ quite considerably by 0.078–0.112 Å (see deposited table), but the relative ordering of the bond lengths mirrors the experimental values found [$d(\text{Te2}–\text{Te8}) > d(\text{Te4}–\text{Te6}) > d(\text{Te3}–\text{Te7})$]. The Te–Te bond distance alternation in the experimentally determined Te_8^{2+} is significant and more pronounced than in the calculated structure. The calculated average bond length is 2.697 Å shorter than the experimental value of 2.725 Å, which is only marginally shorter than the single-bond distance of 2.74 Å.

Experimental and Computed Raman Spectra. The experimental Raman spectra of blue $\text{S}_8(\text{AsF}_6)_2$ and green $\text{Se}_8(\text{AsF}_6)_2$ are given in Figure 10 and Figure 11, respectively. Observed bands are assigned and are summarized in Table 5 and Table 6. Assuming local C_s symmetry for the E_8^{2+} ($E = \text{S}, \text{Se}$)

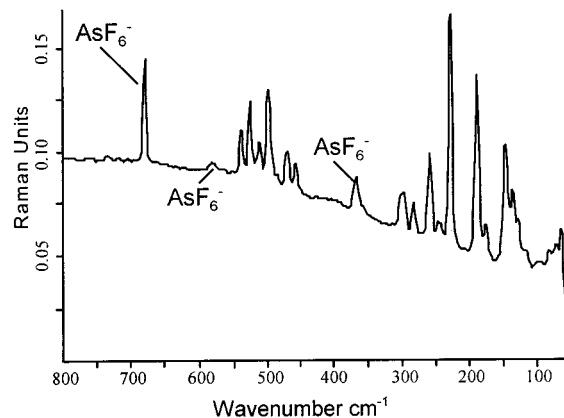


Figure 10. FT-Raman spectrum of blue $\text{S}_8(\text{AsF}_6)_2$ obtained at 150 K in a 5 mm glass tube (300 scans, 4 cm^{-1} resolution, and a 90°, focused, 22 mW laser beam). Apodization function: Norton–Beer, medium. Acquisition mode: double sided, fast return. Scanner velocity: 4 mm/s. Aperture: 12 mm.

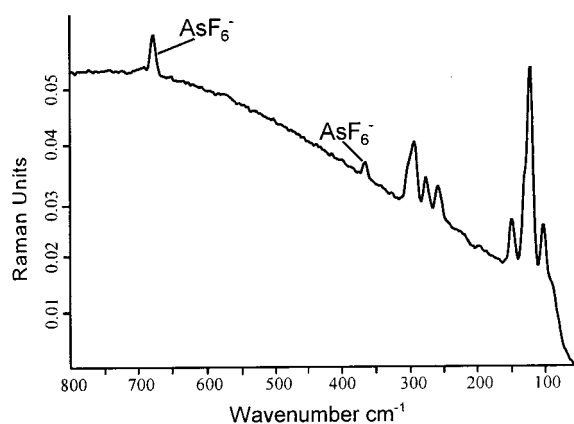


Figure 11. FT-Raman spectrum of green $\text{Se}_8(\text{AsF}_6)_2$ obtained at 150 K in a 5 mm glass tube (300 scans, 4 cm^{-1} resolution, and a 90°, focused, 28 mW laser beam). Apodization function: Norton–Beer, medium. Acquisition mode: double sided, fast return. Scanner velocity: 4 mm/s. Aperture: 12 mm.

dications, 18 vibrational modes of A' (10) and A'' (8) symmetry are anticipated, all being IR and Raman active. Sixteen of these have been observed in $\text{S}_8(\text{AsF}_6)_2$. Different scaling factors for high-energy ($\nu > 300$ cm^{-1} , $f = 1.064$) and low-energy ($\nu < 300$ cm^{-1} , $f = 1.051$) vibrations were derived by scaling the respective calculated frequencies in order to obtain the best fit to the experimental values.⁹³ This high-energy scaling factor matched that found in the computation of the tetrasulfur dication at the same level of theory^{20,21} and appears to remain constant for the homopolyatomic cations of sulfur.⁹⁴ Experimental and calculated agreement is excellent. Since the nature of the transannular bonding in S_8^{2+} is in question, a thorough assignment of a (presumably low-energy) vibrational stretching mode between S3 and S7 is essential in order to verify the presence or absence of such an interaction. Raman bands around 250–269 cm^{-1} were assigned corresponding to S–S distances of 2.43–2.55 Å. In S_8O a S–S stretching frequency of 320 cm^{-1} was assigned to the long S–S bond adjacent to the S–O unit [$d(\text{S}–\text{S}) = 2.202$ Å]. Inspection of the calculated vibrational frequencies of the S_8^{2+} dication reveals the presence of a S3–

(88) Optimization with frozen Se3–Se7 distance, MPW1PW91/3-21G*.

(89) It is noted that the classically σ -bonded homopolyatomic cations also have positive charge delocalization as shown for I_3^+ and the second excited state of S_4^{2+} with a butterfly structure, and the polymeric $(\text{Te}_4^{2+})_n$.

(90) Beck, J.; Muller-Buschbaum, K. *Z. Anorg. Allg. Chem.* **1997**, 623, 409.

(91) Beck, J. *Angew. Chem., Int. Ed. Engl.* **1994**, 33, 163 and references therein.

(92) Beck, J. *Coord. Chem. Rev.* **1997**, 163, 55–70 and references therein.

(93) This is the range attributed to S–S stretching (>300 cm^{-1}) and bending (<300 cm^{-1}) modes, see ref 28 for details.

(94) It reflects the overestimation of the S–S bond lengths at the B3PW91/6-311+G* level of theory (1.7–2.0%).

Table 5. Experimental and Calculated (B3PW91/6-311+G*) Frequencies (cm^{-1}) for the S_8^{2+} Dication

exptl ^{a,b} (int %)	theor (scaled) ^c	sym	assignment ^d
536 (35)	541	A'	str 5-6
524 (40)	516	A'	str 4-5, 5-6, bend 4-5-6
510 (30)	515	A'	str 4-5, bend 3-4-5
496 (50)	491	A'	str 7-6(+), 3-4(-), bend 5-6-7, 6-7-8
468 (30)	486	A''	str 3-4, 6-7, and 7-8, bend 3-4-5, 5-6-7, 6-7-8
457 (20)	451	A'	str 3-4, 6-7, bend 3-4-5, 6-7-8
368 (10)	359	A''	str 3-4(+), 7-8(-), bend 2-3-4(+), 3-4-5(+), 5-6-7(-), 6-7-8(-)
298 (32)	303	A'	str 2-3(+), 3-4(+), 7-8(-), bend 2-3-4(+), 3-4-5(+), 6-7-8(-)
282 (20)	292	A''	str 3-7(+), 3-4(-), 7-8(-), bend 2-3-4, 6-7-8
258 (40)	270	A''	bend 1-8-7, 2-3-4, 6-7-8
246 (10)	250	A'	str 7-8, bend 2-1-8(-), 2-3-4(-), 1-8-7(+)
228 (93)	217	A'	str 1-8, bend 2-3-4, 6-7-8, 1-8-7
188 (100)	180	A'	str 1-2, bend 1-2-3, 2-3-4, 1-7-8
176 (20)	165	A''	str 2-3, bend 1-2-3, 2-1-8
146 (80)	146	A''	bend 1-2-3, 2-3-4, 2-1-8
133 (sh)	128	A'	bend 2-1-8 asym
	104	A'	bend 1-2-3, 1-7-8
	88	A''	bend 2-1-8 sym

^a Observed for blue $\text{S}_8(\text{AsF}_6)_2$ at 150 K. ^b $\nu_{\text{sym}}(\text{AsF}_6^-) = 678 \text{ cm}^{-1}$.

^c Scaled by 1.064 ($\nu > 300 \text{ cm}^{-1}$) or 1.051 ($\nu < 300 \text{ cm}^{-1}$), see text.

^d (+) = strong, (-) = weak contribution.

Table 6. Experimental and Calculated (MPW1PW91/3-21G*) Frequencies (cm^{-1}) for the Se_8^{2+} Dication

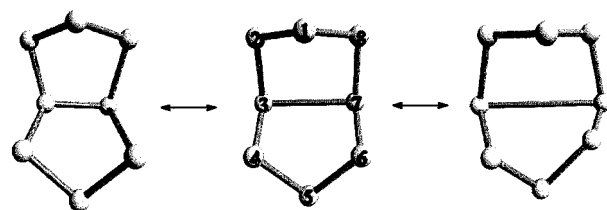
exptl ^{a,b} (int %)	theor (scaled) ^c	sym	assignment ^d
	343	A'	str 4-5, 5-6, bend 4-5-6
	327	A'	str 1-2, 1-8, 4-5, 5-6, bend 2-3-4, 6-7-8
	322	A''	asym str 3-4, 6-7, 4-5, 5-6, bend 2-3-4, 6-7-8, 4-5-6
	318	A'	sym str 3-4, 6-7, 4-5, 5-6, bend 3-4-5, 5-6-7, 4-5-6
305 sh (30)	303	A''	asym str 2-3, 7-8, 1-2, 1-8, bend 2-1-8, 2-3-4, 6-7-8
296 (60)	297	A'	sym str 2-3, 7-8, 1-2, 1-8, bend 1-2-3, 7-8-1
278 (30)	281	A''	asym str 1-2, 1-8, 4-5, 5-6
260 (27)	256	A'	asym ring str of all adjacent atoms
	180	A''	str 2-3(-), 3-4(-), 6-7(-), 7-8(-), bend 2-3-4(+), 6-7-8(+)
152 (50)	148	A'	bend 1-2-3(+), 7-8-1(+), 2-3-4(-), 6-7-8(-)
sh	130	A'	str 3-7, bend 2-1-8, 4-5-6
sh	128	A'	str 3-7, bend 3-4-5, 5-6-7, 2-1-8, 4-5-6
125 (100)	125	A''	asym ring bend, 2,3,4,6,7,8 moving
105 (30)	102	A'	str 3-7, bend 2-1-8, 4-5-6
(90? sh)	94	A''	str 2-4, 6-8, bend 2-3-4, 6-7-8
(90? sh)	92	A'	str 3-7, bend 2-1-8, 4-5-6, 1-2-3, 7-8-1, 3-4-5, 5-6-7
	56	A''	sym ring bend, all atoms
	48	A''	asym ring bend, all atoms

^a Observed for green $\text{Se}_8(\text{AsF}_6)_2$ at 150 K. ^b $\nu_{\text{sym}}(\text{AsF}_6^-) = 678 \text{ cm}^{-1}$.

^c Scaled by 1.021 ($\nu > 200 \text{ cm}^{-1}$) or 0.971 ($\nu < 200 \text{ cm}^{-1}$), see text.

^d (+) = strong, (-) = weak contribution.

S7 stretching mode at 292 cm^{-1} (scaled, exptl: 282 cm^{-1}) which includes some smaller stretching contributions from the S3-S4 and S7-S8 stretches. A graphic representation of the two end points, together with the relaxed position of this vibration, is given in Figure 12. The experimentally observed frequency

**Figure 12.** Graphic representation of the end points of the calculated transannular S3-S7 stretching mode at 282 cm^{-1} (exptl; calculated, scaled: 292 cm^{-1} B3PW91/6-311+G*).

of 282 cm^{-1} for this transannular stretching mode occurs at higher energy than the respective bands found in the sulfur nitrogen cages and bicycles,³⁹ although these exhibit shorter (and therefore stronger) S-S bonds compared to the ones found in S_8^{2+} . In these S-N species the next neighbors to the sulfur atoms are the lighter nitrogen atoms. The force constants of the S-S and S-N stretching modes are very different, and the S-S stretches in these S-N species are, therefore, relatively isolated. In the S_8^{2+} we do not find an isolated transannular stretch, but instead a combination with contributions from the short (and high-energy) S3-S4 and S7-S8 bonds. Consequently this vibration is found at higher energy when compared to the more isolated S-S stretching modes as are found in the S-N cages.

In the Raman spectrum of green $\text{Se}_8(\text{AsF}_6)_2$ all of the observed vibrational frequencies occur between 340 and 90 cm^{-1} . Only six of the 18 fundamental modes of the Se_8^{2+} dication were unambiguously observed, three more as shoulders (see Figure 11). To derive scaling factors for the MPW1PW91/3-21-G* level of theory, only the six vibrational modes at 105 , 125 , and 152 cm^{-1} (bends) and those at 260 , 278 , and 296 cm^{-1} (stretches) were employed. The high-energy (low-energy) scaling factor followed as 1.021 (0.971). Calculated scaled and observed frequencies agree to within $\pm 4 \text{ cm}^{-1}$. The calculated bands at 128 and 130 cm^{-1} are assigned as symmetric and antisymmetric transannular Se3-Se7 stretching modes with some additional bending contributions. This assignment compares well to the observed weak Se-Se stretching frequencies in the experimental spectra of Se_3Cl_3^+ and Se_3Br_3^+ .⁵⁴ Long Se-Se bond distances of 2.551 (Se_3Cl_3^+) and 2.558 \AA (Se_3Br_3^+) were found in the solid state, which correspond to Se-Se stretching frequencies of 162 (Se_3Br_3^+) and 174 cm^{-1} (Se_3Cl_3^+). In Se_8^{2+} the transannular distance is about 2.84 \AA , and therefore we observe a stretching mode which is lower in energy at about 130 cm^{-1} . Se_3Br_3^+ offers a good comparison, since Se and Br have almost the same weight (78.96 vs 79.90), and therefore mixed vibrations are found rather than more isolated Se-Se stretches observed in Se_3Cl_3^+ ⁵⁴ or Se_4N_4 .⁹⁵ The cross ring E3-E7 stretching modes in E_8^{2+} (E = S, Se) provide strong evidence for the presence of transannular bonding, not withstanding the mixed nature of the vibration.

The Clusterlike Bonding in E_8^{2+} (E = S, Se)

The annular bond distances in E_8^{2+} imply bond orders that are slightly higher than 1 around the eight-membered ring. The transannular distances are all in the region of 2.86 – 3.00 \AA (S_8^{2+}) and 2.84 – 3.35 \AA (Se_8^{2+}) and raise the question as to which are bonding interactions and which are not, i.e., which of the valence structures **1**, **2**, and **3**, in Figure 2, are significant. The NBO⁶⁹ analysis (Figure 13) showed that the annular bonds have Wiberg bond orders slightly greater than 1 when calibrated

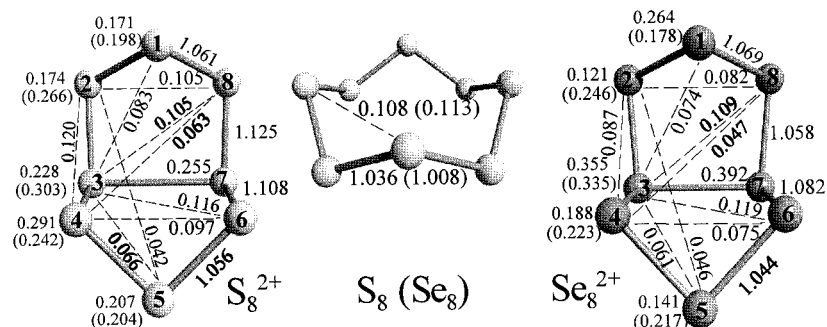
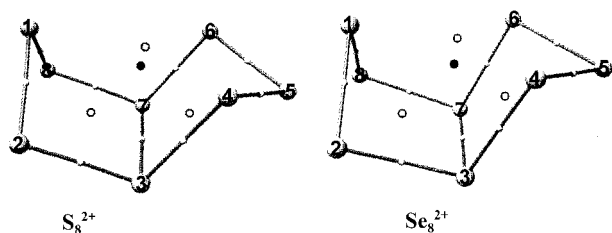


Figure 13. Bonding in E_8^{2+} : Experimental valency units (calculated natural charges within parentheses) on the left of the S_8^{2+} and Se_8^{2+} structures. Calculated Wiberg bond orders are given within the structure and on the right (symmetry equivalent values are omitted). Sum of sulfur (selenium) vdW radii: 3.70 (3.90) Å. Sulfur (selenium) bond distances: $d(2-8)$ 3.017 (3.202) Å, $d(3-7)$ 2.873 (2.776) Å, $d(4-6)$ 2.990 (3.220) Å, $d(1-3)$ 3.204 (3.456) Å, $d(1-4)$ 3.526 (3.600) Å, $d(2-4)$ 3.276 (3.522) Å, $d(3-8)$ 3.583 (3.770) Å, $d(3-6)$ 3.576 (3.766) Å, $d(3-5)$ 3.107 (3.385) Å.



- ↔ = AIM bond critical point
- = AIM ring critical point
- = AIM cage critical point

Figure 14. Calculated (AIM)⁷⁰⁻⁷⁴ bond, ring, and cage critical points in S_8^{2+} and Se_8^{2+} .

against the Wiberg bond order for S_8 and Se_8 .⁹⁶⁻⁹⁸ It also showed that by far the most important cross ring interaction is E3–E7 corresponding to the shortest cross ring bond length, and consistently E3 and E7 have the highest experimental (valency units)^{75,99} and calculated atomic charges. The AIM analysis¹⁰⁰ (Figure 14, more complete information is given in the Supporting Information) showed that there are AIM⁷⁰⁻⁷³ bond critical points between all atoms in the ring framework, and one transannular bond critical point between E3–E7 showing unambiguously that it is a bond. This is supported by corresponding stretching frequencies for this bond in the Raman spectrum (see above and Figure 12). However, the experimental and calculated charges on all of the other atoms are significant and imply that the valency of these atoms is greater than 2 (i.e., sulfur with a charge of +1 has a valency of 3). The total charge on the rings is +2; therefore, there are nine bonds formed per ring, including an extra bond formed on removal of an electron

(96) It is noted that according to this treatment there is some weak bonding between all nonadjacent atoms by a $p^2 \rightarrow \sigma^*$ interaction. However only annular AIM bond critical points are detected, as well as a ring critical point. This and related molecules warrant further study.

(97) Bond orders smaller than 0.02 are omitted in Figure 13.

(98) The NBO analysis provides the polar coordinates of the orientation of the calculated position of the p-type lone pairs. The polar coordinates of two points on the vector through the lone pair that are ± 1 Å apart from the nucleus were converted into xyz coordinates. These xyz coordinates were then visualized together with those of the S_8^{2+} dication with the help of the program RESVIEW.⁶³

(99) The valency units of the Se_8^{2+} dication were not previously published. We calculated those for the salt $Se_8(AlCl_4)_2$ from the published atomic coordinates and the derived distances of the $Se \cdots Cl$ contacts of each individual Se atom according to ref 75 where $R_0 = 2.167$ Å and $N = 4.0$.

(100) We note that Bader et al.⁷² have carried out an AIM analysis of S_8^{2+} . However the level of theory (RHF/STO-3G) gives a much shorter transannular bond (2.22 Å) than observed experimentally [2.905(3) Å] for S_8^{2+} , leading to a classical view of the bonding.

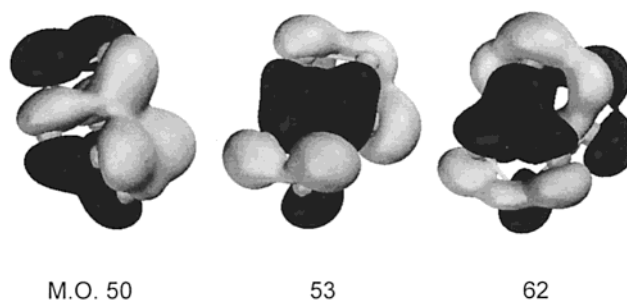


Figure 15. Graphic representations of the three clusterlike molecular orbitals number 50 (HOMO-13), 53 (HOMO-10), and 62 (HOMO-1) in S_8^{2+} (MPW1PW91/3-21G*) (isosurface drawn at 0.042 au).

from the filled p^2 orbitals of neutral E_8 . A portion of this bond is to be found as partial annular π bonding, and some in the E3–E7 bond. The NBO analysis showed weak interactions between the other atoms (Figure 13). The AIM analysis (Figure 14) showed a cage critical point (electron density increases in all directions from this point), and ring critical points for the two fused five-membered rings and one for the whole E_8 ring, confirmed by tracing the gradient paths of the electron density from the ring critical points to the bond critical points using the new AIM2000 program.^{74,101} The Wiberg bond orders for the E1–E4 contacts were both about 0.015. It may be that there is an interaction between the partially filled p^2 orbitals, as shown in Figure 22, leading to some very weak bonding between E1 and E4, E6, but with greater total electron density buildup in this region than the net bond order suggests. The cage-like bonding in E_8^{2+} is supported by the clusterlike occupied MO's, as shown in Figure 15 for sulfur; the selenium case is similar and therefore not included. Very weak bonding between E1 and E4, E6 favors the formation of the observed exo–endo structure which is lower in energy by 38 kJ/mol than the less stable crown S_8 -like exo–exo isomer. However there is less Coulombic repulsion between positively charged E atoms (NBO and Mulliken charges and geometries [UB3PW91/6-311+G(d)], details deposited) in the observed exo–endo structure.

The structure of E_8^{2+} (E = S, Se, Te) may also be understood in terms of an electron deficient Wade–Mingos cluster.¹⁰²⁻¹⁰⁵ Banister¹⁰⁶ made a proposal of this kind some years ago and attempted to deduce the S_8^{2+} geometry starting from an

(101) A full AIM analysis of S_8^{2+} is in progress.

(102) Wade, K. *Adv. Inorg. Chem. Radiochem.* **1976**, *18*, 1.

(103) Mingos, D. M. P. *Acc. Chem. Res.* **1984**, *17*, 311.

(104) Mingos, D. M. P.; Slee, T.; Zhengyang, L. *Chem. Rev.* **1990**, *90*, 383.

(105) Rudolph, W. *Acc. Chem. Res.* **1976**, *9*, 446.

(106) Banister, A. J. *Nature, Phys. Sci.* **1972**, *239*, 69.

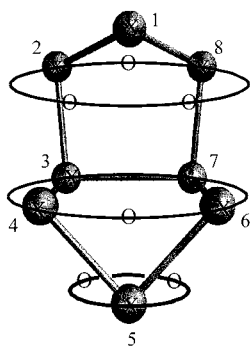


Figure 16. The structure of E_8^{2+} (E = S, Se, Te) as an $n + 6$ type Wade–Mingos cluster incorporated in a 14-cornered polyhedron derived from an icosahedron by replacing the lower cap by a triangle. X symbolizes occupied corners, and O stands for unoccupied corners.

octahedron. E_8^{2+} has 46 valence electrons (VE). The ns^2 electrons ($n = 3, 4, 5$) are inert and occupy eight ns^2 lone pair orbitals (=16 VE, see NBO analyses above). The remaining 30 p-type electrons ($46 - 16 = 30$ VE) are utilized for the formation of the actual structure, or, in other terms, 15 bonding skeleton electron pairs (=SEP) are used for this (in agreement with Banister's assignment¹⁰⁶). Since the parent polyhedron of a Wade–Mingos cluster^{102–105} always has one corner less than the number of SEP, we assume that a polyhedron with 14 corners is required to derive the E_8^{2+} structure. This is an $n + 6$ type ($n = \text{number of corners} = 8$, which requires $n + 7 = 15$ SEP) and thus lies beyond the n (closo), $n + 1$ (nido), $n + 2$ (arachno), and $n + 3$ (hypho) nomenclature as given by Wade and Mingos. If one replaces the lower cap of an icosahedron (12 corners) by a triangle, this leads to a 14-cornered polyhedron¹⁰⁷ which accommodates and explains all structural features of E_8^{2+} (see Figure 16, the belts of the two five- and one three-membered rings are indicated by circles). The E3–E7 bond occupies adjacent positions within these five-membered rings [thus $d(E3-E7)$ is comparatively small] whereas the E2–E8 and E4–E6 atom pairs are each separated by one (unoccupied) corner in these rings. This explains their greater separation and shows that this model works best for the heavier homologues with larger differences between the lengths of the E3–E7 and the E2–E8 or E4–E6. All of these homopolyatomic cations comprise an ensemble of nearly similarly charged atoms.¹⁰⁸ In order to minimize the Coulombic repulsion and to maximize the positive charge delocalization (i.e., to minimize the overall energy), these species occupy a portion of the surface of a regular polyhedron as in the Wade–Mingos electron deficient cluster theory.^{102–105} This also implies that molecular cluster orbitals are formed, as found above for E_8^{2+} . The sulfur atoms in the observed exo–endo S_8^{2+} are more nearly on the surface of a sphere than is the less stable¹⁰⁹ exo–exo S_8^{2+} isomer (details deposited). The sum of the Coulombic repulsion energy between positively charged atoms is more in the less stable exo–exo S_8^{2+} isomer. This implies that the shape of E_8^{2+} is governed by the minimization¹⁰⁹ of electrostatic Coulombic repulsion by the maximization of positive charge delocalization which (as one possible description) is achieved by the formation of an $n + 6$ type Wade–Mingos cluster having 15 SEP.

(107) It is recognized that this polyhedron is not a deltahedron but possesses one square face (all other faces are triangular). However, it is assumed that there is nearly no difference in energy between this 14-cornered polyhedron and a pure triangularly faced 14-cornered deltahedron.

(108) See the experimental or NBO charges in Figure 13.

(109) The exo–exo S_8^{2+} isomer is 38 kJ/mol higher in energy than clusterlike exo–endo S_8^{2+} [B3PW91/6-311G(2df)//B3PW91/6-311+G*]. Details are included in the Supporting Information.

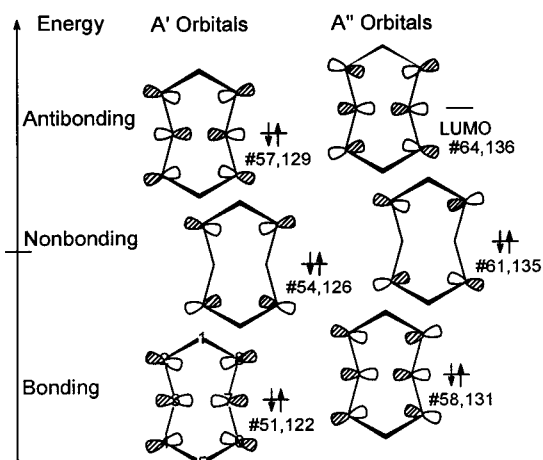


Figure 17. The six molecular orbitals of A' and A'' symmetry, of E_8^{2+} (E = S, Se), formed by the six partially occupied np^2 lone pair orbitals ($n = 3, 4$) and the respective number of the calculated orbitals at the MPW1PW91 level of theory (#number). Orbital 57 (129) is a representation of the proposed intramolecular $\pi^*-\pi^*$ bond. A' orbitals are bonding across the ring; A'' orbitals are antibonding.

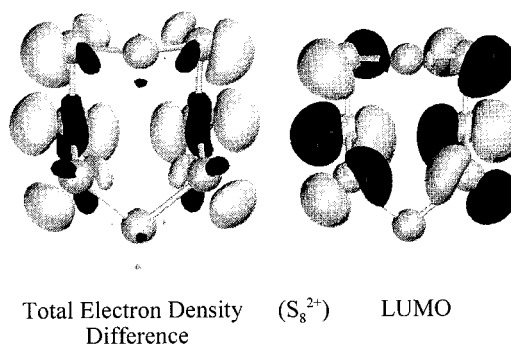


Figure 18. The LUMOs (orbital #64) of S_8^{2+} and the total electron density difference of S_8 and S_8^{2+} (both in the C_s symmetric S_8^{2+} minimum geometry) at the MPW1PW91/3-21G* level of theory (isosurface of the LUMO drawn at 0.042 au). Lighter shaded areas represent electron density left over from S_8 while the darker shaded areas represent electron density left over from S_8^{2+} .

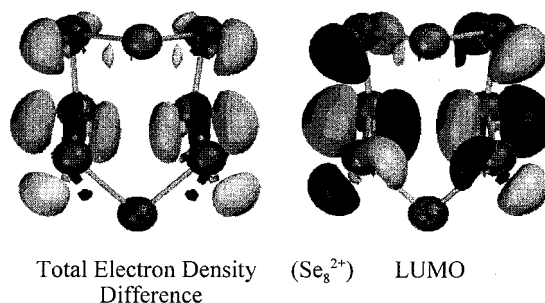


Figure 19. The LUMO (orbital #126) of Se_8^{2+} and the total electron density difference of Se_8 and Se_8^{2+} (both in the C_s symmetric Se_8^{2+} minimum geometry) at the MPW1PW91/3-21G* level of theory (isosurface of the LUMO drawn at 0.042 au). Lighter shaded areas represent electron density left over from Se_8 while the darker shaded areas represent electron density left over from Se_8^{2+} .

A Molecular Orbital Based Understanding of the Bonding in E_8^{2+}

The location of the bond formed on oxidation of E_8 to E_8^{2+} may be inferred from the LUMO of E_8^{2+} and by the electron density difference between E_8 (with the geometry of E_8^{2+}) and E_8^{2+} , as shown in Figures 18 and 19. This implies a charge of about 0.33 on all E2, 3, 4, 6, 7, 8 atoms, a π bond delocalized

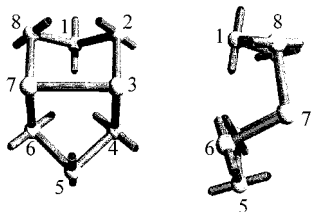


Figure 20. Two views of the calculated position of the NBO $3p^2$ lone pairs at S1, 2, 4, 5, 6, 8 drawn with a length of 1.0 Å.

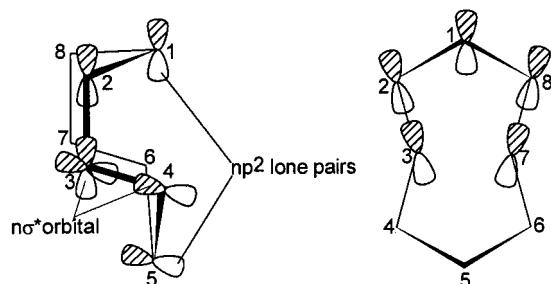


Figure 21. Two views of the $np^2 \rightarrow n\sigma^*$ bond ($n = 3, 4, 5$) as formed by the np^2 lone pairs at E1,5 and the respective E2-3, E7-8, E4-5, or E6-7 $n\sigma^*$ orbitals.

in the ring over these atoms, and three weak transannular $\pi^* - \pi^*$ interactions as shown in Figure 3. The observed E2-E3, E3-E4, E6-E7, E7-E8 bond orders are less than the expected bond order of 1.25 as the dihedral angles between the np orbitals on S2, 4, 6, 8 (Se2, 4, 6, 8) vs the E3-E7 bond are 47.1° and 48.4° (42.8° and 47.1°) (see Figure 20), but still allow some π bonding.^{110,111} The transannular overlap of the np orbitals between E3 and E7 is good but poor between E2 and E8 and between E4 and E6, leading to bent and weak bonds. Shortening of the latter bonds would compress the already acute E2-E1-E8 and E4-E5-E6 bond angles [exptl $92-94^\circ$ (S), $89-92^\circ$ (Se)]. This bonding model given above is supported by the presence of a triplet state S_8^{2+} (see Figure 7) which is only 54 kJ/mol higher in energy than the ground state, i.e., to the first order of approximation S_8^{2+} contains two π^* electrons that pair via a weak intracationic transannular $\pi^* - \pi^*$ interaction. Delocalization of positive charge onto the apical atoms, and thus onto all atoms (average 0.25), is accomplished by donation of the np^2 lone pair electrons into the vicinal E2-E3, E7-E8, and E3-E4, E7-E6 empty $n\sigma^*$ orbitals; a representation of one set of these bonds is given in Figure 21. This stabilizes the system by 28–32.9 (S) and 26.4–32.9 (Se) kJ/mol, respectively (NBO analysis, Figure 23). This increases the π bonding in E1-E2, E1-E3, E5-E4, and E5-E6 and decreases it in E3-E2, E3-E4, E7-E6, and E7-E8. This accounts for the approximately equal E-E bond distances around the E_8^{2+} rings. A similar interaction was first found by Steudel in a number of molecules including $S_7^{47,112}$ and cyclic sulfur imides,¹¹³ and this interaction is responsible for the lengthening of the chalcogen-chalcogen bonds adjacent to a formally positively charged tricoordinated chalcogen atom, e.g. in cations of the type

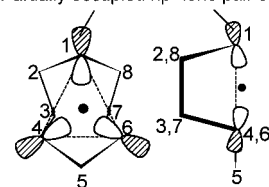
(110) The calculated positions of the NBO $4p^2$ lone pairs in Se_8^{2+} are equivalent to those found in S_8^{2+} depicted in Figure 20, and its representation is therefore omitted. Compared to the S_8^{2+} dication, all of the dihedral angles in Se_8^{2+} differ by less than 5° , and the respective dihedral angles are given in the text.

(111) The np^2 lone pairs at E1, 5 and the neighboring np^2 lone pairs ($n = 3, 4$) are nearly orthogonal (dihedral angle, S, 81.3° and 79.7° ; Se, 79.8° and 81.1°).

(112) Steudel, R. *Top. Curr. Chem.* **1981**, 102, 149.

(113) Drozdova, Y.; Steudel, R. *Phosphorus, Sulfur Silicon Relat. Elem.* **1997**, 124 and 125, 521.

Partially occupied np^2 lone pair orbitals



● = calculated AIM ring critical point

Figure 22. Bonding interaction of the partially occupied np^2 lone pair orbitals ($n = 3, 4, 5$) at E1, E4, and E6.

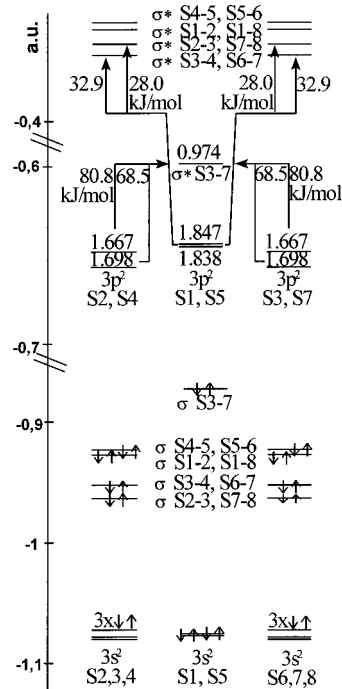


Figure 23. The bonding in the S_8^{2+} dication as derived from the NBO analysis⁶⁹ employing the localized natural bond orbitals. The antibonding $3\sigma^*$ orbitals are occupied by 0.060–0.113 electrons (totaling 0.754); the six partially occupied $3p^2$ lone pair orbitals amount to 10.416 electrons. Bonding σ orbitals are occupied by 1.93–1.98 electrons, respectively. The MO diagram of Se_8^{2+} is very similar (see text).

$Hal_2E^+ - E - EHal$ ($E = \text{chalcogen}$; $Hal = Cl, Br$).^{45,54} The torsion angle between calculated (NBO) position of the np^2 lone pair orbitals ($n = 3, 4$) at E1 and E5 with the E2-E3, E7-E8 or E3-E4, E6-E7 $n\sigma^*$ orbital is $8.7-14.7^\circ$ (S) and $9.9-12.6^\circ$ (Se), verifying the possibility of this $np^2 \rightarrow n\sigma^*$ bond (in Figure 21). This situation shortens the bonds around E1 and E5 and increases bond distances around E3 and E7. Interaction between the np^2 orbitals on E1, E4, and E6, as illustrated in Figure 22, may also occur, leading to weak bonding. The net result is a σ and weakly π bonded annular E_8 framework, a weak σ E3-E7 bond, and other weak interactions. Thus the bonding is highly delocalized as indicated by the MO's shown in Figure 15 and supports the thesis that the bonding in E_8^{2+} is clusterlike.

A Comparison of the Bonding in E_8^{2+} ($E = S, Se, Te$)

The structures of all three cations are similar and imply similar bonding. However, the E3-E7 bond order increases from sulfur to tellurium, i.e., the importance of the classical localized valence bond structure **1** (Figure 2) increases $S \rightarrow Se \rightarrow Te$, whereas the annular π bonding decreases $S \rightarrow Se \rightarrow Te$. There is a corresponding increase of positive charge localization on E3 and E7 (Figure 13).¹¹⁴ The ring E-E bonds are all essentially equal in Se_8^{2+} , but the bonds adjacent to the apical atoms are

Table 7. Dissociation Reactions of E_8^{2+} and $E_8(AsF_6)_2$ ($E = S, Se$) in the Gas Phase and the Solid State, Respectively (Values in kJ/mol)^a

eq.	Dissociation Reactions and $\Delta_f H^\ominus$ of all Reactants [kJ/mol]				$\Delta_f H^\ominus$	
		$E_8^{2+} (g) \rightarrow 2 E_4^+ (g)$				
(6a) $E = S$	$\Delta_f H^\ominus =$	2151	972*		-207	
(6b) $E = Se$	$\Delta_f H^\ominus =$	2071	960*		-151	
		$E_8(AsF_6)_2 (s) \rightarrow 2 E_4AsF_6 (s)$				
(6c) $E = S$	$\Delta_f H^\ominus =$	-3122	-1457		+208	
(6d) $E = Se$	$\Delta_f H^\ominus =$	-3197	-1447		+303	
		$E_8^{2+} (g) \rightarrow E_3^+ (g) + E_5^+ (g)$				
(7a) $E = S$	$\Delta_f H^\ominus =$	2151	1076	939	-136	
(7b) $E = Se$	$\Delta_f H^\ominus =$	2071	1083*	982	-6	
		$E_8(AsF_6)_2 (s) \rightarrow E_3AsF_6 (s) + E_5AsF_6 (s)$				
(7c) $E = S$	$\Delta_f H^\ominus =$	-3122	-1361	-1473	+288	
(7d) $E = Se$	$\Delta_f H^\ominus =$	-3197	-1331	-1402	+464	
		$E_8^{2+} (g) \rightarrow E_2^+ (g) + E_6^+ (g)$				
(8a) $E = S$	$\Delta_f H^\ominus =$	2151	1031	971	-149	
(8b) $E = Se$	$\Delta_f H^\ominus =$	2071	1004	996	-71	
		$E_8(AsF_6)_2 (s) \rightarrow E_2AsF_6 (s) + E_6AsF_6 (s)$				
(8c) $E = S$	$\Delta_f H^\ominus =$	-3122	-1433	-1427	+262	
(8d) $E = Se$	$\Delta_f H^\ominus =$	-3197	-1447	-1380	+370	
		$E_8^{2+} (g) \rightarrow E_2^+ (g) + 0.5 [E_5^+ (g) + E_7^+ (g)]$				
(9a) $E = S$	$\Delta_f H^\ominus =$	2151	1031	939	951	-175
(9b) $E = Se$	$\Delta_f H^\ominus =$	2071	1004	982	962	-95
		$E_8(AsF_6)_2 (s) \rightarrow E_2AsF_6 (s) + 0.5 [E_5AsF_6 (s) + E_7AsF_6 (s)]$				
(9c) $E = S$	$\Delta_f H^\ominus =$	-3122	-1433	-1471	-1437	+235
(9d) $E = Se$	$\Delta_f H^\ominus =$	-3197	-1447	-1402	-1402	+348
		$E_8^{2+} (g) \rightarrow 0.5 E_4^{2+} (g) + E_6^+ (g)$				
(10a) $E = S$	$\Delta_f H^\ominus =$	2151	2318	971		-21
(10b) $E = Se$	$\Delta_f H^\ominus =$	2071	2207	996		+29
		$E_8(AsF_6)_2 (s) \rightarrow 0.5 E_4(AsF_6)_2 (s) + E_6AsF_6 (s)$				
(10c) $E = S$	$\Delta_f H^\ominus =$	-3122	-3104	-1427		+143
(10d) $E = Se$	$\Delta_f H^\ominus =$	-3197	-3182	-1380		+226
		$E_8^{2+} (g) \rightarrow 0.5 [E_4^{2+} (g) + E_5^+ (g) + E_7^+ (g)]$				
(11a) $E = S$	$\Delta_f H^\ominus =$	2151	2318	939	951	-47
(11b) $E = Se$	$\Delta_f H^\ominus =$	2071	2207	982	962	+5
		$E_8(AsF_6)_2 (s) \rightarrow 0.5 [E_4(AsF_6)_2 (s) + E_5AsF_6 (s) + E_7AsF_6 (s)]$				
(11c) $E = S$	$\Delta_f H^\ominus =$	-3122	-3104	-1471	-1437	+116
(11d) $E = Se$	$\Delta_f H^\ominus =$	-3197	-3182	-1402	-1402	+204

^a (*) See text.

slightly longer in S_8^{2+} . This may reflect an increase in $np^2 \rightarrow n\sigma^*$ bonding (Figure 21) for selenium. By extrapolation of the trends observed between S_8^{2+} and Se_8^{2+} , the bonds adjacent to the apical atoms are expected to be the shortest in Te_8^{2+} . This is the case for the bonds to Te1 but not Te5 (Figures 9 and 24). The annular π bonding and stronger transannular bonding is restricted to the Te3, 4, 6, 7 plane. The Te_8^{2+} case is likely more complex: the framework is more flexible as evidenced by the existence of three isomers,^{87,90–92} the cation–anion interactions are stronger for tellurium than the lighter elements, and np^2 – np^2 interactions are likely to increase in importance.

Gas Phase and Solid State Dissociation Behavior of E_8^{2+} and $E_8(AsF_6)_2$ ($E = S, Se$)

The enthalpies of possible dissociations of the parent dication E_8^{2+} into smaller fragments can be calculated once the standard enthalpies of formation $\Delta_f H^\ominus[E_8^{2+}, g]$ ($E = S, Se$) are computed, since the standard enthalpy of formation of gaseous $S_4^{2+}(g)$ of 2318 kJ/mol^{20,21} and the accurate, experimentally determined

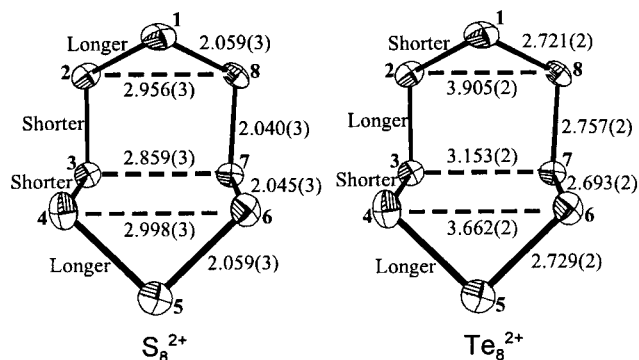


Figure 24. Observed bond lengths (averaged assuming local C_2 symmetry) and bond length alternation in the isostructural E_8^{2+} dications in $S_8(AsF_6)_2$ and $Te_8(ReCl_6)$.

standard enthalpies of formation of the gaseous polychalcogen monocations E_n^+ ($n = 2-7$)^{16,17} are known (see Table 7).

$\Delta_f H^\ominus[E_8^{2+}, g]$ ($E = S, Se$). In earlier studies, employing optimized geometries differing greatly from the experimental geometries, values of 2208 (HF/3-21G*),^{14,18} 2194 (HF/6-31G*),^{14,18} 2093 (HF/6-311G*),⁴⁸ 1975 (BLYP/6-311G*),⁴⁸ and 1947 kJ/mol (MP2/6-311G*)⁴⁸ have been reported for the sum

(114) Hirshfeld charges for Te_8^{2+} . Full charges on atoms given in deposited Table.

of the first and second ionization energies of $S_8(g)$.⁴⁸ A double ionization potential of 1972 kJ/mol for $Se_8(g)$ is reported at the uncorrelated HF/TZVP level of theory,⁴⁸ whereas the correlated MP2/TZVP method gives a value of 1807 kJ/mol.⁴⁸ The underlying trend in these calculations is evident: increasing the size of the basis set lowers the combined ionization potentials obtained considerably; the same holds true for the inclusion of approximate electron correlation by BLYP or MP2. In a preceding investigation^{20,21} of S_2^+ and S_4^{2+} , we showed that the MP2 level of theory greatly overestimates electron correlation when describing homopolyatomic sulfur species. Ionization potentials much lower than the ones observed are therefore computed, whereas uncorrelated HF methods give consistently higher ionization potentials (and closer to the experimental value than MP2). Therefore we take the MP2 values of 1947 (S) and 1807 (Se) kJ/mol as a lower limit and the HF/6-311G* values of 2093 (S) and 1972 (Se) kJ/mol as an upper limit, and presumably closer to the true value. Accordingly one might expect the accurate combined first and second adiabatic ionization potential of neutral octasulfur (octaselenium) to be in the region of 2030 (1900) kJ/mol. This is in agreement with the values obtained by one of us (R.J.D.) in the initial optimization at the B88P86/DZ(d,f) level [$^{1st+2nd}IP(S_8) = 1999$ kJ/mol, $^{1st+2nd}IP(Se_8) = 1857$ kJ/mol]. The successful modeling of the geometries of neutral E_8 and (low-symmetry) dicationic, exo-endo E_8^{2+} reported here lends high credibility to the determination of the combined first and second ionization potential of E_8 , using the B3PW91 or MPW1PW91 level of theory combined with a flexible basis set. Calculated cyclooctasulfur double ionization potentials with the B3PW91/6-311+G*, B3PW91/6-311G(2df), and MPW1PW91/3-21G* geometries are summarized in a deposited table (including the zero-point energy and corrected to 298 K). Our initial computation of the double ionization potential of neutral Se_8 with the B88P86 method gave a value of 1857 kJ/mol which further increased to 1901 kJ/mol when using the MPW1PW91 and a flexible basis set [6-311+G-(3df), see deposited table, including the zero-point energy and corrected to 298 K].

Inspection of the data (deposited) reveals that the inclusion of polarizing f functions is necessary for the accurate description of the energetics of this process. It changes the calculated potential by roughly 60 (S_8 , B3PW91) to 120 (Se_8 , MPW1PW91) kJ/mol. However, diffuse functions (indicated by “+”) and a third set of polarizing d functions only reduce the combined first and second ionization potential of E_8 by 1–4 kJ/mol, indicating that the computation is close to the basis set limit. Values calculated with the B3PW91 and MPW1PW91 level of theory and the largest basis sets agree to within 7 kJ/mol (sulfur). This further increases the confidence in the calculated ionization potential of 2050 (S) and 1901(Se) kJ/mol obtained with the largest basis set and the best geometry [S_8 , B3PW91/6-311+G-(3df)/B3PW91/6-311G(2df); Se_8 , MPW1PW91/6-311+G(3df)/MPW1PW91/3-21G*], close to the estimates derived above. The standard enthalpy of formation of gaseous S_8 $\Delta_f H^\ominus[S_8, g]$ has been determined experimentally to be 101 kJ/mol.^{16,17} Thus we conclude that the standard enthalpy of formation of the gaseous dication S_8^{2+} is given by

$$\Delta_f H^\ominus[S_8^{2+}, g] = \Delta_f H^\ominus[S_8, g] + ^{1st+2nd}IP[S_8, g, 298 K]$$

$$\Delta_f H^\ominus[S_8^{2+}, g] = 101 + 2050 = 2151 \text{ kJ/mol}$$

Using the ionization potential of 1901 kJ/mol calculated with the largest basis set [MPW1PW91/6-311+G(3df)] and the

Table 8. Calculated Electron Affinity (EA) and Ionization Potential (IP) of Atomic Fluorine and Calculated Dissociation Energy of F_2

level of theory	EA(F) ^a	IP(F) ^a	$\Delta H_{\text{diss}}(F_2)^a$
experiment	328	1681	154.8 ± 4
MPW1PW91/6-311+G(3df)	310.07	1690.99	137.38
MPW1PW91/Aug-cc-vPQZ	313.89	1688.17	141.49
B3PW91/6-311+G(3df)	321.36	1700.26	150.16
G96LYP/6-311+G(3df)	242.44	1704.90	191.74
B3LYP/6-311+G(3df)	221.02	1713.96	150.87
HF/6-311+G(3df)	115.13	1514.99	-149.32
MP2/6-311+G(3df)	341.34	1669.50	164.90
MP3/6-311+G(3df)	287.99	1660.28	106.99
MP4(SDQ)/6-311+G(3df)	304.58	1659.87	120.09
QCISD(T)/6-311+G(3df)	290.70	1664.97	141.08

^a In kJ/mol.

published standard enthalpy of formation of gaseous neutral Se_8 of 170 kJ/mol,^{16,17} we obtain the standard enthalpy of formation of Se_8^{2+} (g, 298 K) to be

$$\Delta_f H^\ominus[Se_8^{2+}, g] = \Delta_f H^\ominus[Se_8, g] + ^{1st+2nd}IP[Se_8, g, 298 K]$$

$$\Delta_f H^\ominus[Se_8^{2+}, g] = 170 + 1901 = 2071 \text{ kJ/mol}$$

No previous reports of the calculation of the combined first and second ionization potential of Te_8 are available. Following the trends as observed for S and Se a lower IP is expected and found. The combined first and second ionization potential of $Te_8(g)$ at 0 K without zero-point energy correction is 1666 kJ/mol [B88P86/DZ(d,f)], rendering the cation much less electrophilic than the lighter homologues [cf. $^{1st+2nd}IP(S_8)$, 2050; $^{1st+2nd}IP(Se_8)$, 1901 kJ/mol]. However, the enthalpy of formation of gaseous Te_8 is not known and therefore $\Delta_f H^\ominus[Te_8^{2+}, g]$ cannot be established. Since Te_8 is less stable than Se_8 and S_8 , it is likely that $\Delta_f H^\ominus[Te_8, g]$ will be higher than the one found for $Se_8(g)$ (170 kJ/mol) giving 1936 kJ/mol as the lower limit for $\Delta_f H^\ominus[Te_8^{2+}, g]$. Adding the same difference as observed between S_8 and Se_8 (170 – 101 = 69 kJ/mol) leads to a rough estimate of $\Delta_f H^\ominus[Te_8^{2+}, g]$ to be 2005 kJ/mol.

The Fluoride Ion Affinity of AsF_5 and $\Delta_f H^\ominus[AsF_6^-, g]$. The standard enthalpy of formation of gaseous AsF_6^- is needed to assess the thermodynamics of solid hexafluoroarsenate salts of the gas phase dissociation reactions of E_8^{2+} . Two different values for this enthalpy of formation are published in the literature. In the first estimate $\Delta_f H^\ominus[AsF_6^-, g]$ is calculated on the basis of the estimate by Bartlett et al. of the fluoride ion affinity (FIA) of AsF_5 as 467 kJ/mol [$AsF_5(g) + F^-(g) \rightarrow AsF_6^-(g)$].⁵¹ From this value and $\Delta_f H^\ominus$ of -255 and -1234 kJ/mol for $F^-(g)$ ¹¹⁵ and $AsF_5(g)$,¹¹⁶ respectively, $\Delta_f H^\ominus[AsF_6^-, g]$ is found to be -1953 ± 17 kJ/mol. Recently we (H.D.B.J. and J.P.)⁵² estimated $\Delta_f H^\ominus[AsF_6^-, g]$ using the thermochemical data for the salts $[NF_4^+][BF_4^-]$, $[NF_4^+][SbF_6^-]$, and $[NF_4^+][AsF_6^-]$ leading to a value of -1919 ± 43 kJ/mol, which is 34 kJ/mol lower than Bartlett's value. Therefore this lower standard enthalpy of formation implies a lower fluoride ion affinity of AsF_5 of 433 kJ/mol. To decide which value (433 or 467 kJ/mol) is likely to be the more accurate, we modeled the fluoride ion affinity using ab initio methods (B3PW91 and MPW1PW91) and concluded to a most likely value of 430.5 ± 5.5 kJ/mol (for details see ref 117 and Tables 8 and 9).

Although the published fluoride ion affinity of SbF_5 is identical to Bartlett's FIA of AsF_5 (467 kJ/mol),⁵¹ SbF_5 is known

(115) Gurvich, L. V.; Veyts, I. V.; Alcock, C. B. *Thermodynamic Properties of Individual Substances*, 4th ed.; Hemisphere: New York, 1989.

(116) O'Hare, P. A. G. *J. Chem. Thermodyn.* **1993**, 25, 391.

Table 9. Calculated and Experimental Geometries of AsF_5 and AsF_6^- and Calculated Fluoride Ion Affinity (FIA) of Gaseous AsF_5

property	exptl ^a	MPW1PW91/ 6-311+G(3df)	B3PW91/6-311+G(3df)// MPW1PW91/6-311+G(3df)
AsF_5 : $d(As-F_{ax})^b$	1.711(6)	1.703	
AsF_5 : $d(As-F_{eq})^b$	1.656(6)	1.680	
AsF_6^- : $d(As-F)^b$	1.713(7)	1.740	
FIA[AsF_5 , g], ^{c,d}		436	425
FIA[AsF_5 , g], ^{c,e}		422	419

^a Not corrected for librational motion. ^b In Å. ^c In kJ/mol. ^d Using $F^- + AsF_5 \rightarrow AsF_6^-$. ^e Using $OCF_3^- + AsF_5 \rightarrow O=CF_2 + AsF_6^-$ and FIA[$O=CF_2$] = 209 kJ/mol.

to be a stronger acceptor than AsF_5 . Consequently one might anticipate obtaining a higher FIA for SbF_5 as is found in Christe's and Dixon's recent calculations¹¹⁹ which give a FIA- $[SbF_5, g]$ of 503 kJ/mol and our thermochemical estimation of the FIA of $SbF_5(l)$ of 521 kJ/mol.⁵² This and the calculated FIA of gaseous AsF_5 of 430.5 ± 5.5 kJ/mol suggest that the lower fluoride ion affinity of AsF_5 of 433 kJ/mol^{49–52} is more accurate and thus $\Delta_f H^\ominus[AsF_6^-, g]$ of -1919 ± 43 kJ/mol is used for estimating the solid state thermodynamics of $E_8(AsF_6)_2$ (E = S, Se).

Thermodynamics in Gaseous and Solid Phases. The solid state behavior of the respective gas phase dissociation reactions in Table 7 were assessed by estimating the lattice potential energies of the hexafluoroarsenate salts of the respective S_n^+ monocations by using our generalized equation.^{49,50} To verify the quality of this estimate, the lattice energy of $S_8(AsF_6)_2$ was derived as follows: The standard enthalpy of formation of $S_8(AsF_6)_2(s)$ has been determined experimentally by fluorine bomb calorimetry as -3122 ± 12 kJ/mol,¹⁸ and therefore the lattice potential enthalpy of $S_8(AsF_6)_2$ can be derived according to

(117) It is well-known that the energies of fluorine-containing compounds are difficult to model accurately.¹¹⁸ Therefore we performed simple test calculations [to obtain the electron affinity (exptl: 328.0 kJ/mol) and ionization potential (exptl: 1681 kJ/mol) of atomic fluorine, and the dissociation energy of F_2 (exptl: 154.84 kJ/mol)]^{16,17} using a variety of levels and the large 6-311+G(3df) basis set in order to establish the quality of the different methods. The HF, MP2, MP3, MP4, QCISD(T), B3LYP, and G96LYP levels of theory performed moderately well to very poorly and reproduced at least one of the above experimental values with an error greater than 40 (up to 220) kJ/mol, shown in Table 8. Therefore these methods were not used for our determination of the fluoride ion affinity of AsF_5 . However, the B3PW91 and MPW1PW91 levels of theory [using the 6-311+G(3df) basis set] consistently reproduced all three properties with a maximum error of $-20/+19$ kJ/mol. A recalculation employing the even larger AUG-cc-pVQZ basis set [80 basis functions per fluorine atom vs 39 in 6-311+G(3df)] only decreased the maximum error by 2–4 kJ/mol, indicating that the calculation using the 6-311+G(3df) basis set must be close to the basis set limit (see Table 8). Therefore the B3PW91/6-311+G(3df) and MPW1PW91/6-311+G(3df) levels of theory were selected to determine the fluoride ion affinity (FIA) of arsenic pentafluoride, AsF_5 (D_{3h} symmetry), AsF_6^- (O_h symmetry), and F^- were fully optimized at the MPW1PW91/6-311+G(3df) level of theory. Their computed geometries are in very good agreement with the experimentally determined gas phase structure of AsF_5 and X-ray crystal structure determinations of the undistorted AsF_6^- anion, i.e., in $KAsF_6$ (see Table 9). Both methods agree within 11 kJ/mol on a value of 430.5 ± 5.5 kJ/mol for the fluoride ion affinity of AsF_5 (see Table 9), close to the value of 433 kJ/mol of Jenkins and Passmore.⁴⁹ This is further supported by the recent results of K. Christe and D. Dixon.¹¹⁹ They calculate the FIA of AsF_5 at the MP2/DZP level to be 443 kJ/mol. For completeness, we repeated this procedure using the hybrid-HF-DFT levels but found only small changes (see Table 9). Since the calculation of the electron affinity, ionization potential, and dissociation energy involves open- and closed-shell species, these values are often difficult to mirror computationally.¹²⁰ In the calculation of the fluoride ion affinity of AsF_5 only properties of closed-shell species were examined (F^- , AsF_5 , AsF_6^- , $O=CF_2$, OCF_3^-) so increasing the confidence in the quality of this computation.

$$U_{\text{POT}}[S_8(AsF_6)_2] + 3RT = \Delta_f H^\ominus[S_8^{2+}, g] + 2\Delta_f H^\ominus[AsF_6^-, g] - \Delta_f H^\ominus[S_8(AsF_6)_2, s] \quad (5)$$

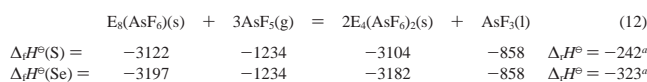
With the thermochemical value for $\Delta_f H^\ominus[AsF_6^-, g]$ of -1919 ± 43 kJ/mol the lattice potential enthalpy of $S_8(AsF_6)_2$ according to eq 5 is found to be 1434 ± 55 kJ/mol. Estimation of this lattice enthalpy using our generalized equation^{49,50} and the unit cell volume of $S_8(AsF_6)_2$ derived from the X-ray crystal structure determination yields the lattice potential enthalpy as 1455 kJ/mol, well within the standard deviation of the “semi”-experimentally derived value of 1434 ± 55 kJ/mol. Knowing the experimental standard enthalpies of formation of gaseous polysulfur radical cations S_n^+ ($n = 2-7$),^{16,17} the derived $\Delta_f H^\ominus[AsF_6^-, g]$ and the estimated¹²¹ lattice potential enthalpies of all $S_n AsF_6$, the standard enthalpies of formation of solid $S_n AsF_6$ were then calculated. These values enable us to estimate $\Delta_f H^\ominus(s)$ for possible gas phase dissociations of S_8^{2+} [using the experimental¹⁸ enthalpy of formation of $S_8(AsF_6)_2$ and our recent value of $\Delta_f H^\ominus[S_4^+, g]$.¹²² In order to compare the gas phase and solid state dissociation pattern of $S_8(AsF_6)_2$ and $Se_8(AsF_6)_2$, a similar approach was followed for the selenium homologues.¹²⁵ All values were obtained for 1 mol of crystalline salt at room temperature and are cited below the respective formulas in Table 7.

As can be seen from Table 7 (eqs 6ab–9ab), $E_8^{2+}(g)$ (E = S, Se) is unstable toward dissociation to all the stoichiometrically possible combinations of E_n^+ ($n = 2-7$). Further, all dissociation processes are considerably less favored for Se_8^{2+} than for S_8^{2+} . The most favored dissociation (apart from eq 6ab) is given in

- (118) See, for example: Hehre, W. J.; Radom, L.; Pople, J. A.; Schleyer, P. v. R. *Ab Initio Molecular Orbital Theory*; Wiley-Interscience: New York, 1986.
- (119) (a) Christe, K.; Dixon, D. Presented at the 14th Winter Fluorine Chemistry Conference, 1999, St. Petersburg, FL; Abstract 22. (b) Christe, K. O.; Dixon, D. A.; McLemore, D.; Wilson, W. W.; Sheehy, J.; Bootz, J. A. *J. Fluorine Chem.* **2000**, *101*, 151. (c) Dixon, D. A. Private discussion with H.D.B.J., October 2000.
- (120) Due to the quartet contamination in the one-electron approximation of the wave function of the open-shell species.
- (121) Volumes employed in our generalized equation of ref 50 (respective lattice enthalpies of the AsF_6^- salts in kJ/mol): 110 \AA^3 for AsF_6^- , S_8^{2+} 180 \AA^3 (based on X-ray, 1462), S_4^{2+} 84 \AA^3 (1584), S_2^+ 45 \AA^3 (545), S_3^+ 79 \AA^3 (518), S_4^+ 90 \AA^3 (510), S_5^+ 122 \AA^3 (479), S_6^+ 146 \AA^3 (479), S_7^+ 166 \AA^3 (469). [Ion volumes estimated assuming $Br_2^+ > S_2^+ > SN^+$; $Br_3^+ > S_3^+ > Cl_3^+$, $S_3N_2^+ > S_4^+ > S_4^{2+}$; $Br_5^+ > S_5^+ > S_3N_2^+$; $S_3Br_3^+ > S_6^+ > S_5^+$, $S_7I^+ > S_7^+ > S_4N_3^+$].
- (122) Earlier we showed^{20,21} that the published appearance potential of S_4 (and the associated standard enthalpy of formation of S_4^+) is due to the fragmentation of neutral S_6 giving S_4^+ and S_2 . In agreement with earlier theoretical investigations^{123,124} we established the standard enthalpy of formation of gaseous S_4^+ to be 972 kJ/mol, 159 kJ/mol more favorable than the previously published, erroneously assigned value of 1131 kJ/mol. Consequently we utilize in this work the lower value of 972 kJ/mol for $\Delta_f H^\ominus[S_4^+, g]$.
- (123) Zakrzewski, V. G.; Niessen, W. von *Theor. Chim. Acta* **1994**, *88*, 75.
- (124) Quelch, G. E.; Schaefer, H. F.; Marsden, C. J. *J. Am. Chem. Soc.* **1990**, *112*, 8719.
- (125) However, the ionization potentials and standard enthalpies of formation of gaseous Se_3^+ and Se_4^+ are not available. Published appearance potentials stem from the fragmentation of larger neutral allotropes,¹²⁶ analogous to S_4^+ . Therefore the standard enthalpy of dissociation of Se_8^{2+} to yield $2Se_4^+$ was calculated.¹²⁷ Similarly the standard enthalpy of formation of Se_3^+ was obtained at the same level.¹²⁸ The standard enthalpies of formation for Se_n^+ ($n = 2, 5, 6, 7$) were taken from the literature,^{16,17} and the standard enthalpy of formation of gaseous Se_4^{2+} was derived from the published^{20,21} dimerization energy of 199 kJ/mol for the process $2Se_2^+ = Se_4^{2+}$ and the experimental standard enthalpy of formation of gaseous Se_2^+ (g) of 1004 kJ/mol. Solid state standard enthalpies of formation of the respective hexafluoroarsenate salts were obtained using reasonable estimates for the volumes of the ions¹²⁹ in our generalized equation.⁴⁹

eq 9ab and implies the presence of the dichalcogen radical cation E_2^+ . However, we recently showed that 2 equiv of the solid E_2AsF_6 salt ($E = S, Se$) are not stable toward dimerization into $S_4(AsF_6)_2 [Se_4(AsF_6)_2]$ by 238 [291] kJ/mol.⁸² Consequently, dissociation reactions by formation of the resulting diamagnetic S_4^{2+} dication are also included in Table 7 (eqs 10ab–11ab). These dissociations are favored for $E = S$ (by 21–47 kJ/mol) but not for selenium (by 5–29 kJ/mol). A dissociation of E_8^{2+} (g) by formation of two E_4^+ (g) cations is the most exothermic reaction (S , 207 kJ/mol; Se , 151 kJ/mol). Such a route of dissociation was proposed in the first experimental report¹¹ on $S_8(AsF_6)_2$ in order to provide an explanation for the paramagnetic nature of solutions of this salt. In the solid state (eqs 6cd–11cd), $S_8(AsF_6)_2 [Se_8(AsF_6)_2]$ is always favored by at least 116 [204] kJ/mol (eq 6b). Since the formation of Se_4^{2+} is not favored in the gas phase, only the dissociation reactions of $Se_8(AsF_6)_2$ by the formation of the respective monocations should be taken into account (eqs 6d to 9d) and $Se_8(AsF_6)_2$ is then favored by at least 303 kJ/mol. Thus the $E_8(AsF_6)_2$ salts are further^{130,131} examples of compounds where the parent dication is not stable in the gas phase and the solid state structure is lattice enforced. Analysis shows that this arises because the lattice energy of the 2:1 salt is approximately 3 times greater than that of the respective 1:1 salt.¹³²

The oxidation of $E_8(AsF_6)_2$ ($E = S, Se$) with arsenic pentafluoride (eq 12) was assessed using $\Delta_f H^\circ[AsF_5, g] = -1234$ kJ/mol, $\Delta_f H^\circ[AsF_3, l] = -858$ kJ/mol,^{16,17} and the standard enthalpies of formation of $S_4(AsF_6)_2(s)$ (–3104 kJ/mol), $S_8(AsF_6)_2(s)$ (–3122 kJ/mol), $Se_4(AsF_6)_2(s)$ (–3182 kJ/mol), and $Se_8(AsF_6)_2(s)$ (–3197 kJ/mol).



^a In kJ/mol.

Reaction 12, an often employed preparation of $E_4(AsF_6)_2$, is exothermic by 242 (S) or 323 (Se) kJ/mol, in good agreement

- (126) Berkowitz, J.; Chupka, W. A. *J. Chem. Phys.* **1966**, *45*, 4289.
 (127) Se_4^+ (D_{4h} symmetry) was fully optimized at the MPW1PW91/3-21G* level of theory and is a true minimum, $d(Se-Se) = 2.319$ Å. Energies given were computed at the MPW1PW91/6-311G(2df)//MPW1PW91/3-21G* level, include the zero-point energy, and are corrected to 298 K.
 (128) The geometries of Se_3 and Se_3^+ (C_{2v} , employing the minima found previously for S_3 and S_3^+)^{122–124} were fully optimized at the MPW1PW91/3-21G* level of theory and are true minima. Se_3 : $d(Se-Se) = 2.188$ Å, $Se-Se-Se = 115.5^\circ$. Se_3^+ : $d(Se-Se) = 2.195$ Å, $Se-Se-Se = 95.2^\circ$. Energies given were computed at the MPW1PW91/6-311G(2df)//MPW1PW91/3-21G* level, include the zero-point energy, and are corrected to 298 K. Thus the ionization potential of Se_3 is calculated (938 kJ/mol). The enthalpy of formation of gaseous Se_3 is calculated from the experimental enthalpy of formation of gaseous Se_8 (170 kJ/mol) and the subsequent calculated enthalpy of reaction of $3/8 Se_8(g) = Se_3(g)$ (145 kJ/mol). Thus we conclude to a gaseous enthalpy of formation of Se_3^+ of 1083 kJ/mol.
 (129) Volumes employed in our generalized equation of ref 50 (respective lattice enthalpies of the AsF_6^- salts in kJ/mol): 110 Å³ for AsF_6^- , Se_8^{2+} 214 Å³ (1430), Se_4^{2+} 94 Å³ (1551), Se_2^+ 59 Å³ (532), Se_3^+ 114 Å³ (495), Se_4^+ 127 Å³ (488), Se_5^+ 175 Å³ (465), Se_6^+ 196 Å³ (457), Se_7^+ 230 Å³ (445). (Ion volumes estimated assuming $I_2^+ > Se_2^+ > S_2^+$; $I_3^+ > Se_3^+ > Br_3^+$; $SeI_3^+ > Se_4^+ > Se_4^{2+}$; $I_5^+ > Se_5^+ > Se_3NCl_2^+$; $Se_6^+ > Se_6^{2+} > Se_3Br_3^+$. Se_7^+ ion volume found from extrapolation of Se_n^+ .)
 (130) A further example for a lattice-stabilized species is the $S_3N_2^{2+}$ dication, which dissociates in the gas phase to give SN^+ and S_2N^+ ($\Delta H = -400$ kJ/mol), but is present in the salt $S_3N_2(AsF_6)_2$, see ref 131.
 (131) Brooks, W. V. F.; Cameron, T. S.; Parsons, S.; Passmore, J.; Schriver, M. J. *Inorg. Chem.* **1994**, *33*, 6230.

with experimental experience, although for $E = S$ the reaction only proceeds in the presence of a trace halogen X_2 ($X = Cl, Br, I$)^{76,81} and for $E = Se$ only with prolonged heating.

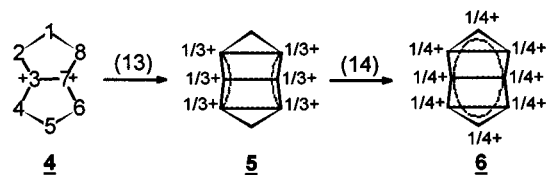
Conclusion

Crystals of $S_8(AsF_6)_2$ that are red in transmitted light were prepared, providing direct evidence that S_8^{2+} is not blue. A low-temperature X-ray structure was obtained more accurately than hitherto^{11,44} and the data corrected for librational motion.

Satisfactory calculated geometries of gaseous E_8^{2+} ($E = S, Se$) depend on the inclusion of an accurate description of electron correlation. These species have been successfully modeled and mirror all observed properties [best computations: B3PW91/6-311G(2df) (S); MPW1PW91/6-311G(2df) (Se)]. The E3–E7 bond lies in a very shallow potential well. This explains earlier problems experienced in attempting to obtain correct geometries.^{47,48} The new MPW1PW91 level of theory provides a well-balanced description of electron correlation so that even the 3-21G* basis set is sufficient to model the geometry of S_8^{2+} and Se_8^{2+} . This knowledge will enable us to investigate larger systems such as E_{10}^{2+} , E_{17}^{2+} , and E_{19}^{2+} ($E = S, Se$). Calculations aiming to model thermochemical properties of the E_8^{2+} dications must use flexible basis sets. The inclusion of at least two sets of polarizing d functions and one set of polarizing f functions appears to be the minimum needed to obtain satisfactory values [=6-311G(2df)]. E_8^{2+} ($E = S, Se$) are unstable in the gas phase and dissociate in a number of equilibria to radical cations E_n^+ ($n = 2-7$) and/or the dication S_4^{2+} (see Table 7). The most favorable gas phase dissociations of E_8^{2+} ($E = S, Se$) yield $2E_4^+$ and $E_2^+ + 0.5[E_5^+ + E_7^+]$ in keeping with the experimental observation of at least two radicals (S_5^+ and probably S_7^+)^{12,13,19} in solutions of $S_8(AsF_6)_2$ and also raises the question as to whether other sulfur radical cations can be experimentally detected.

An AIM analysis of the bonding in E_8^{2+} ($E = S, Se$) showed (Figure 14) that there are bonds between all atoms in the E_8 ring, one transannular bond, for which a Raman stretch is observed, and a cage critical point from which the electron density increases in all directions. The NBO and AIM analysis, and an examination of the molecular orbitals, showed that the extra bond formed on oxidation of E_8 to E_8^{2+} is highly delocalized, increasing the bond order of the annular bonds to slightly more than 1, and leading to other weak bonds, the strongest of which is the E3–E7 transannular bond. The positive charge is delocalized over all atoms, decreasing the Coulombic repulsion between positively charged atoms relative to that in the less stable S_8 -like exo–exo E_8^{2+} isomer. The overall geometry was accounted for by the Wade–Mingos rules, further supporting the case for cage bonding.^{102–105} The bonding in Te_8^{2+} is similar, but with a stronger transannular E3–E7 ($E = Te$) bonding. The bonding in E_8^{2+} ($E = S, Se, Te$) can also be understood in terms of a σ -bonded E_8 framework with additional bonding and charge delocalization occurring by a combination of transannular $n\pi^* - n\pi^*$ ($n = 3, 4, 5$), and $np^2 \rightarrow n\sigma^*$ bonding. The classically bonded structure **4**, e.g., $[E_2(CH_2)_6]^{2+}$ ($E = S, Se$, see Table 1),³⁴ with localized charges residing on E3 and E7 is not observed, but rather charge is delocalized to E2, E3, E4, E6, E7, and E8 (**5**) by formation of a six-center intramolecular $\pi^* - \pi^*$ bond which includes weak cross ring interactions (eq 13) as well as $np_\pi - np_\pi$ ($n \geq 3$) bonds. In addition, positive

- (132) Compare to the Kapustinskii treatment of the lattice potential energy which is proportional to the number of ions and the charge of the species, e.g., a factor of 2 is found for an A^+B^- salt but one of 6 for an $A^{2+}(B^-)_2$ salt.



charge is transferred onto E1 and E5 (see Figures 17, 18, 19) by delocalization of an np^2 lone pair at E1 and E5 into the formally empty no^* orbitals (see Figure 21) corresponding to the E2–E3, E3–E4, E6–E7, and E7–E8 bonds (**6**, eq 14). This weakens these bonds but strengthens the remaining adjacent bonds with the formation of some $np_\pi-np_\pi$ ($n \geq 3$) bonding. The fully delocalized structure **6** of S_8^{2+} (Se_8^{2+}) is 29 (6) kJ/mol lower in energy than the localized isomer **4**.

Acknowledgment. We thank the Natural Sciences and Engineering Research Council (NSERC) of Canada (J.P., I.K.), the EPSRC (H.K.R.), the Alexander von Humboldt Foundation in Bonn, Germany, for providing a Feodor-Lynen Fellowship (I.K.), Dr. Holger Schwenk for the use of his *RESVIEW* program, Dr. Friedrich Grein, UNB, for many useful discussions and assistance during the course of this work, and Dr. Ron Gillespie and Dr. Paul Popelier for many useful comments on the AIM analysis. Jesus College, Oxford, is acknowledged with

gratitude for a Senior Visiting Research Fellowship during which (1996/1997, J.P.) the foundation for this paper was established and Prof. A. J. Downs is thanked for his hospitality.

Supporting Information Available: An X-ray crystallographic file for $S_8(AsF_6)_2$ (CIF). Tables S1–S7, complete crystallographic details, atomic coordinates and anisotropic displacement parameters for $S_8(AsF_6)_2$, bond distances, bond and torsion angles, and nonbonded contacts. Table S8, computed and experimental structural parameters of S_8 and exo–endo S_8^{2+} . Table S9, comparison of the results from the NBO analysis of S_8^{2+} with three geometries. Tables S10 and S11, comparison of the computed and experimental structural parameters of Se_8 , Se_8^{2+} , and Te_8^{2+} . Table S12, comparison of the computed and experimental cross ring bonding (\AA) in E_8^{2+} ($E = S, Se$). Tables S13 and S14, AIM properties for S_8^{2+} and Se_8^{2+} : charge densities ρ (au), Laplacians of the charge densities $\nabla^2\rho$ (au) at the critical points, and bond ellipticities ϵ . Tables S15 and S16, details of calculated deviation of the atoms in the exo–exo and exo–endo S_8^{2+} isomers from positions on a sphere and total calculated Coulombic repulsion energy between atoms (NBO and Mulliken charges) for both isomers. Tables S17 and S18, combined first and second adiabatic ionization potentials of S_8 and Se_8^{2+} . Figure S1, comparison of new and published structures of S_8^{2+} . Figure S2, a view of the unit cell along the monoclinic axis. Figure S3, comparison of the published structures of Se_8^{2+} . This material is available free of charge via the Internet at <http://pubs.acs.org>.

IC990760E